NASA TECHNICAL NOTE

NASA TN D-1953

NASA TN D-1953

EVALUATION OF AN ELECTROMAGNETIC SHOCK TUBE FOR GENERATING STRONG SHOCKS IN AIR

by James F. Roach;
Langley Research Center,
Langley Station, Hampton, Va.

NATIONAL AERONAUTICS AND SPACE ADMINISTRATION • WASHINGTON, D.C. • OCTOBER 1963

TECHNICAL NOTE D-1953

EVALUATION OF AN ELECTROMAGNETIC SHOCK TUBE FOR GENERATING STRONG SHOCKS IN AIR

By James F. Roach

Langley Research Center
Langley Station, Hampton, Va.

NATIONAL AERONAUTICS AND SPACE ADMINISTRATION

NATIONAL AERONAUTICS AND SPACE ADMINISTRATION

TECHNICAL NOTE D-1953

EVALUATION OF AN ELECTROMAGNETIC SHOCK TUBE FOR GENERATING STRONG SHOCKS IN AIR[1]

By James F. Roach

SUMMARY

An evaluation has been made of the performance of a 3-inch electromagnetic shock tube operated in air. The shocks were driven by the discharge of a high-voltage low-inductance capacitor bank. A rotating-mirror camera was used to examine the highly luminous flow generated by the low-pressure discharge. Luminous front speeds between 0.4 and 4.0 cm/μsec were obtained in a range of initial shock-tube pressures from 10 to 1,000 microns of mercury. The luminous waves were reflected off a downstream plug and the reflected speeds were found to be roughly a factor of 2 greater than those predicted by one-dimensional equilibrium shock theory. Time-integrated spectra of the discharge were obtained in the spectral region 3,500 A to 5,000 A. The flow was found to be very nonuniform, and no definite contact surface could be resolved. It is concluded that the device would be unsuited for controlled aerodynamic studies.

INTRODUCTION

This paper describes the operation and performance of a linear discharge tube for generating strong shocks in air by means of a high-voltage spark. Such a device is set apart from the conventional shock tube in that no diaphragm is employed. Instead, driving conditions are obtained by the discharge of a capacitor bank at one end of an evacuated tube. The ambient gas is thus rapidly heated (on the order of 10^{-6} seconds) by the spark discharge and the subsequent expansion of the hot ionized gas coupled with magnetic driving forces results in the propagation of a highly luminous shock wave down the discharge tube.

In the conventional picture of a shock tube the strength of the shock is increased by increasing the pressure ratio and speed-of-sound ratio across a diaphragm. A high-speed-of-sound ratio is accomplished, for example, by selecting low-molecular-weight driver gases and by direct combustion or electric heating of the driver gases. In the case of the electromagnetic shock tube the driver and driven sections, that is, thinking of the discharge region as the driver

---

[1]Some of the information presented herein was offered as a thesis in partial fulfillment of the requirements for the degree of Master of Arts, College of William and Mary, Williamsburg, Virginia, Aug. 1962.

section and the expansion region as the driven section, are evacuated to the same pressure (and contain the same gas). The shock strength will depend for the most part on the efficiency of the transfer of electric and magnetic energy into thermal energy and volume driving forces on the ionized gas. The immediate advantage of such a device is that, for small tubes on the order of several inches in diameter, it requires only a small energy source on the order of 10^3 joules to generate shock Mach numbers M_S up to approximately 50 in air. On the other hand, because of the transient nature of the discharge and the strong radiant condition of the gas, the shock structure and propagation mechanism may deviate markedly from the hydrodynamic shock model.

The early work on electromagnetic shock tubes began in 1951 when Fowler and Lee (ref. 1) were trying to elucidate the problem of the so-called "Rayleigh afterglow" which appeared in appendages off a main electrical discharge tube. In a later paper by Fowler and others (ref. 2) the now familiar T-tube was used to examine the nature of these luminous fronts. Their results suggested the kinship of these waves with shock waves and large-amplitude acoustical disturbances. In general, they found the luminous-front velocity to be directly proportional to the capacitor energy and inversely proportional to the initial pressure and molecular weight of the gas. They observed that the waves were attenuated and that "echo" or reflected waves were present.

Since the propagating gases were highly ionized, it was suggested that the application of external magnetic fields would increase the driving energy, which previously was derived mainly from joule heating. Kolb (ref. 3) and Kash (ref. 4) modified the T-tube shock generator to include several arrangements of field-coil and "back strap" geometries to apply a Lorentz volume force on the hot ionized gas created by the electric discharge. They were able to increase greatly the luminous front velocity by these means. Josephson (ref. 5) later introduced a linear tapered tube discharge for generating strong axial shocks. In this case the strong "pinching" of the gas by the self-induced magnetic field of the discharge was the major driving force. Shock Mach numbers M_S of approximately 150 in deuterium and approximately 50 in air were readily obtainable in these devices at pressure levels of interest in reentry studies. In addition to the tapered tube (or "pinch" tube) and T-tube generators, several other forms of the electromagnetic shock tube have been reported. A good summary of these devices as well as the development of electromagnetic shock tubes through 1959 may be found in reference 6.

Some recent work at Langley on electromagnetic generation of hypervelocity flows has been directed toward the development of steady-state devices. A continuous-flow electrodeless plasma accelerator was reported in reference 7 and a crossfield accelerator in reference 8. A more comprehensive study of a d-c crossfield accelerator was reported in references 9 and 10. Work on other hypervelocity flow devices has been presented in reference 11. In addition to these steady-state facilities, a pulsed electrodeless discharge apparatus for generating hypervelocity shock fronts was examined in reference 12.

Most research employing these devices and electromagnetic shock tubes has been directed toward the development of preheaters for thermonuclear machines, applications as propulsion devices, and for basic magnetohydrodynamic studies.

Some work has been done on measuring the properties of the ionized gases generated in an electromagnetic shock tube, for example, the electric conductivity measurements of deuterium plasmas in reference 13. Very little work has been reported, however, in applying the flow in these devices to study problems in hypervelocity aerodynamics.

One such study has been carried out by Ziemer (refs. 14 and 15) by using the flow in a tapered-tube type of electromagnetic shock tube. In this study, the effects of an external magnetic field on stagnation aerodynamic heating on a 1-inch hemisphere were examined. Measurements were found to be in agreement with the magnitude of the predicted decrease in the heating rate and increase in bow-wave standoff distance due to the applied magnetic field. A novel thin-film infrared heat-transfer gage was developed to detect the level of the aerodynamic heating and is reported in references 16 and 17.

The present study was initiated in an effort possibly to extend Ziemer's approach with the electromagnetic shock tube to include measurements of radiant-heat-transfer levels to blunt bodies. In this note the performance of an electromagnetic shock tube, similar to Ziemer's device, operated in air at pressures between 10 and 1,000 microns of mercury is reported. A qualitative evaluation is made of the shock flow mainly with the aid of smear camera pictures. It is concluded that the flow generated by this apparatus would be unsuited for controlled quantitative radiant heating studies.

SYMBOLS

C	capacitance of bank, μf
L_e	effective circuit inductance, μh
I_p	peak current defined by $\frac{2\pi V_o C}{T}$, amps
M_s	shock Mach number, ratio of shock velocity to speed of sound in unshocked gas
p_1	initial shock-tube pressure, microns of mercury
R_e	effective circuit resistance, ohms
T	period of discharge, μsec
U_r	luminous-reflected-shock velocity, cm/μsec
U_s	luminous-shock-front velocity, cm/μsec
V_o	initial voltage on capacitor bank, kv
x	distance from exit of shock generator, cm

DESCRIPTION AND OPERATION OF THE ELECTROMAGNETIC SHOCK TUBE

Apparatus

The shock tube is similar to the device used by Ziemer and described in reference 6. General ground rules for the design of the device are found in a recent paper by Josephson and Hales (ref. 18). It is evident from their paper as well as from those of early workers that a low system inductance and high initial current rise time are desirable for generating strong shocks. These general criteria were followed in the present design. Figure 1 shows a photograph of the shock tube and capacitor bank energy source. Figure 2 presents a sketch of the shock tube and schematically indicates the luminous-front history of a shock wave generated by means of the tapered-tube shock generator which is described later.

The essential parts of the apparatus are (1) the coaxial-cable coupling of the capacitors to the discharge region, (2) the atmospheric air-gap switch, (3) the discharge region, (4) the 3-inch-diameter glass pipe, and (5) the vacuum pump.

The capacitor bank consists of nine 1-microfarad capacitors rated at 30 kilovolts at a ringing frequency of 150 kilocycles. The maximum energy storage is 4,050 joules. The bank is coupled to the discharge region by a bundle of 18 coaxial cables, 2 for each capacitor to minimize inductance. The sheaths are terminated by a press fit between 2 brass plates and the center conductors are extended for some 10 inches and then terminated by lugs at the rear of the positive air-gap switch electrode. A second electrode completes the air-gap switch and extends into the low-pressure-discharge region. The circuit is completed by six copper straps, 1/4 inch by 1/32 inch, which are insulated by two layers of electrical tape and passed over the air-gap switch to the sheath termination point.

The shock tube proper is a 3-inch heat-resistant glass pipe. Standard glass fittings were used to fasten the discharge region and end plate to the shock tube. O-rings were used for all vacuum seals. A mechanical vacuum pump was used to evacuate the system to pressures of 10 to 1,000 microns of mercury in air. A 0- to 1,000-micron gage measured the initial shock-tube pressure which was controlled by a Teflon-seat bleed valve. Room air was the testing medium.

Circuit and Air-Gap Switch

A circuit diagram is presented in figure 3. The charging, firing, and shorting phases of the shock-tube operation were controlled by three high-voltage vacuum relay switches. The charging and firing switches are normally open and the shorting switch is normally closed. The shorting and firing resistors are banks of 3-K 160-watt and 5-K 50-watt wire resistors, respectively.

The time of discharge was controlled by an atmospheric air-gap switch. Figure 4 shows a sketch of the switch. The opposing surfaces of the copper electrodes are approximate equipotentials of a parallel plate capacitor for a gap separation of 0.37 inch. Under standard atmospheric conditions this distance should hold off about 30 kilovolts in air. The analysis for this electrode contour is attributed to Rogowski, who calculated the equipotentials at the edge of

a parallel plate capacitor. (See ref. 19.) At the rounded edges of the electrodes the theoretical field strength decreases rapidly as is indicated in the figure. A rubber insulated brass rod is inserted along the axis of the positive electrode and the two electrodes are maintained at the same potential during the charging cycle by the 200-megohm bank of carbon resistors. This setup was to prevent misfirings before the required charging voltage was obtained because of leakage of the high-voltage vacuum firing switch.

This switch has performed very reliably. The eroded area on the surface of the electrodes indicated that the discharge always occurred in the center portion of the gap and that the discharge column was about 3/8 inch in diameter.

Electrode Configurations

Three electrode configurations were used during this investigation. They are sketched in figure 5 and will be referred to throughout this paper as the button-ring, spindle-cone, and pinch-tube configurations. In the first arrangement (fig. 5(a)) a copper ring $2\frac{1}{2}$ inches in length is the ground electrode and a hollow copper button electrode is the positive electrode. The electrode was bored out to reduce electrode erosion. A Bakelite insulator separated the electrodes. In the second configuration (fig. 5(b)) a $7\frac{1}{2}$-inch tapered spindle electrode is placed along the axis of a hollow tapered conical electrode having a 1/8-inch thickness. These electrodes were made of aluminum. The last configuration (fig. 5(c)) is similar to that used by Ziemer in his work with the electromagnetic shock tube. It consists of a solid copper button electrode and the ring electrode used in the first configuration. These electrodes are separated by a section which is constructed of heat-resistant glass and tapers parabolically from 3 inches at the exit end of the discharge to 3/4 inch at the position of the button electrode: a 1-inch precision-bore tubing allows for an O-ring seal with the button electrode.

EXPERIMENTAL RESULTS AND ANALYSIS

Shock Generation

Diagnostic techniques.- The luminous fronts generated by the discharge were analyzed mainly by a rotating mirror camera with writing speeds up to 3 millimeters per microsecond with an air drive. The smear pictures were obtained on black and white 35-millimeter strip film. Qualitative information about the shock flow and structure was obtained by using color film. Time-integrated photographs of luminous phenomena were also useful in understanding the shock flow. A 1/10-microsecond Kerr cell was used in the study of the pinch-discharge mechanism. An oscilloscope and a several-turn field coil placed near the discharge region supplied information about the effective circuit characteristics.

Time-integrated spectra of the discharge were obtained with a grating spectrograph. The dispersion was roughly 16 angstroms per millimeter and allowed spectra to be taken in the first order between 2,350 A and 7,000 A. A concave grating of the replica type having 15,000 lines per inch and a focal length of 53 centimeters was employed.

Electrical characteristics.- The effective circuit parameters were estimated from the ringing frequency and the current decay of the discharge. A small 1/4-inch-diameter 2-turn field coil was used to follow the current discharge. The coil was placed on the center conductor bundle in the case of the button-ring configuration and along the tapered glass section for the pinch tube. No traces were obtained for the spindle-cone configuration. The following typical oscilloscope trace shows the first derivative of the current as a function of time.

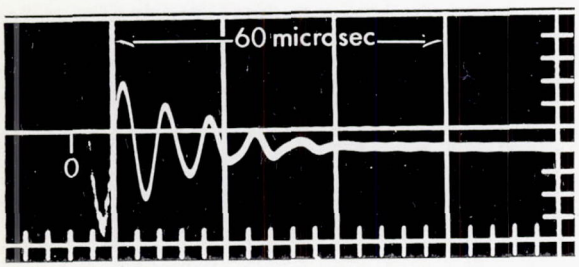

From such traces the effective circuit inductance and resistance were deduced by measuring the period and decay of the signal peaks. The results for the two electrode configurations at different voltage conditions are presented in the following table:

CALCULATED CIRCUIT PARAMETERS FOR TYPICAL OPERATING CONDITIONS

Parameter	Electrode configuration	
	Button-ring	Pinch tube
Charging volts, V_o, kv	12.5	20
Capacitance, C, μf	6	9
Period, T, μsec	6.6	7.5
Effective inductance, L_e, μh	0.18	0.16
Effective resistance, R_e, ohms . . .	0.03	0.03
Peak current, I_p, amps	71,400	151,000

These cases represent roughly the maximum and minimum total energy conditions used in driving the shocks. Most of the external inductance of the system is a result of the air-gap switch arrangement.

Generation of shocks with pinch tube.- Because the button-ring and spindle-cone electrode configurations were not amenable to visual observation, no data were obtained on the mechanism of producing the shocks in these generators. However, in the case of the pinch-tube configuration, the discharge region could be observed visually by removal of one of the ground-return straps. The pinch

discharge was then examined qualitatively with the rotating-mirror camera, time-average photographs, and Kerr cell exposures. The results are shown in figure 6. The photographs are arranged so that the position of the ring electrode (see fig. 5(c)) is situated at the top and that of the button electrode at the bottom in each picture.

The rotating-mirror picture (fig. 6(a)) was obtained by placing a 1/2-inch slit on the tapered glass section along the direction of the shock tube axis. A time history of the lumination appearing in the slit as a function of distance along the slit was then obtained. The smear picture shows that illumination first begins at the button electrode and progresses in time to the ring electrode. Just before reaching the ring electrode, there is a marked increase in the velocity of the front. A second luminous front is observed to follow the primary wave. The dotted lines indicate the positions of these fronts.

Figure 6(b) shows a 1/10-microsecond (Kerr cell) exposure of the discharge during the first microsecond of the current buildup. From this picture one observes in the region of the button electrode a highly luminous "ball." Distinct luminous rays seem to emanate from this ball and proceed to the ring electrode and apparently near the inside wall of the tapered glass section. The hot pencil ray of illumination along the axis in figure 6(c) is not observed during this early stage of the discharge.

The time-average photograph (fig. 6(c)) of the pinch discharge was obtained by reducing the intense light from the discharge by means of two crossed-plane polarized sheets. This picture indicates that the highly luminous discharge seems to be confined in a small column along the tube axis. The width of the column is greater near the button electrode and tapers to a narrow pencil ray of hot gas at the exit of the shock generator.

From the photographs in figure 6, a qualitative description of the pinch-tube driving mechanism is inferred. When the discharge is initiated, the current first flows along the inner wall of the tapered tube. The magnetic field arising from the current flow immediately begins to drive the ionized gas into the axis of the tube. Because the current density and degree of ionization is much larger at the button electrode, this "pinching" is much stronger than at the exit end of the discharge region. The hot gas at the button electrode is then driven along the axis by sequential pinching which adds more energy to the gas. This hot filament of gas "squirts" out of the tapered glass section and expands axially and radially into the uniform glass pipe. Following behind this first traveling filament of hot gas is a second wave of hot gas, which eventually overtakes the primary front farther downstream in the expansion section.

A more complete analysis of a pinch discharge shock driver operated in deuterium has been reported by Josephson and Hales in reference 20. (See also Josephson's original work on the pinch tube, ref. 5.)

Luminous front smears.- Figure 7 shows typical smear pictures of the luminous wave propagation for each of the three electrode configurations. All the pictures indicate that multiple luminous fronts are generated. (These fronts are referred to as secondary waves and the foremost luminous front as the primary

wave.) It is also apparent that the primary front is strongly attenuated at the exit of the discharge region. More specifically, the luminous wave patterns generated by the button-ring configuration (fig. 7(a)) are very complex because of the interactions of the secondary and primary waves. On the other hand, the secondary waves exhibited by the spindle-cone (fig. 7(b)) and pinch-tube (fig. 7(c)) smears follow progressively behind the primary wave and do not catch up with the primary wave until much farther downstream of the discharge exit.

The secondary waves arise from the ringing of the discharge which results in repeated heating of the gas in the discharge region at each current half-cycle. In the case of the button-ring and spindle-cone configurations, the time interval between the appearance of successive multiple waves near the generator exit was roughly that of the half-period of the discharge. Figure 8 shows this correlation for the case of the button-ring configuration for several initial pressures. As many as six secondary waves were observed. This is in agreement with the scope traces of the discharge which indicated that the discharge is completely damped after about 10 half-cycles. In the case of the pinch-tube configuration (fig. 7(c)) only two or three secondary waves were observed.

Performance of the shock generators.- The foremost luminous front velocity was measured from the smear pictures with an accuracy of about ±10 percent. Figure 9 presents the front velocity at several stations downstream of the discharge as a function of the initial shock-tube pressure. (Note: 1 cm/μsec ≈ 32,800 ft/sec.) For each electrode configuration the general behavior of the luminous front propagation was the same. At distances of less than 2 tube diameters from the exit of the generators, velocities in the range of 2 to 4 cm/μsec were obtained. The attenuation of the waves was severe; thus, beyond 5 tube diameters the front velocity was generally less than 1 cm/μsec.

Figure 9 also shows that the luminous front velocity was a complex function of the initial pressure for constant capacitance and charging voltage. Near the exit of the discharge the velocity varied directly with pressure below about 200 μHg. At intermediate distances of about 2 tube diameters the curves indicate a maximum velocity at pressures between 40 and 100 μHg. For a downstream station greater than 8 tube diameters, the velocity was always an inverse function of the initial pressure. The performance curve of the tapered-tube electromagnetic shock tube used by Ziemer (ref. 17) is shown in figure 9(c) for comparison.

Figure 10 illustrates the early attenuation of the luminous front with distance from the generator exit. In the case of the spindle-cone and button-ring configurations, the decay was roughly proportional to x^{-1}, and in the pinch tube, $x^{-1/2}$. For the latter configurations, figure 10(a) also shows the increase in front velocity due to reinforcement by a secondary wave at a distance of about 2.5 tube diameters. Such abrupt increases in the luminous front velocity were not present in the waves generated by the pinch tube where the secondary waves were observed to merge smoothly with the primary front. Reference 21 shows that the attenuation of a one-dimensional blast wave is proportional to $x^{-1/2}$. For a cylindrical and spherical blast wave, the attenuation is respectively proportional to x^{-1} and $x^{-3/2}$. Thus, as the spatial degrees of freedom increase, the attenuation is greater. In the case of the spindle-cone configuration, because of the

small exit area of the conical electrode, one would expect radial expansion of the ejected plasma and attenuation greater than predicted for the one-dimensional case. The large attenuation also exhibited by the button-ring configuration is probably due to nonuniform heating of the spark discharge which generates local plasma blobs that expand radially as well as axially as they are expelled. The very complex pattern of secondary waves generated by this configuration would perhaps indicate mixing and other dissipation processes. On the other hand, in the case of the pinch tube, the attenuation was roughly that expected for a one-dimensional blast wave.

In comparing the shock generators, it is evident that the spindle-cone configuration was the least promising for generating flows which could be maintained well downstream of the discharge region. In fact, the luminous front velocity was already less than 1 cm/μsec at a distance of 2 tube diameters. The button-ring and pinch-tube generators, on the other hand, produced luminous waves with velocities up to 1 cm/μsec at distances of 8 tube diameters from the discharge. The front velocities generated by the button-ring configuration were obtained for an initial capacitor energy storage of 469 joules and in the case of the pinch tube, 1,800 to 3,125 joules. Thus, the driving efficiency, that is, front velocity per total energy storage, of the button-ring configuration was roughly 5 times that of the pinch tube at a distance of 8 tube diameters from the discharge. However, the complex wave pattern exhibited by the button-ring configuration would indicate severe nonuniformities in the flow up to 5 tube diameters.

In the following sections the flow generated in the pinch tube is examined more closely. Shock profiles are presented and the reflection of the luminous waves is discussed. Time-integrated spectra of the discharge are also analyzed.

Comments on Shock Flow Generated by Pinch Tube

Shock profile.- The shock profiles were obtained with the streak camera by placing observation slits perpendicular to the tube axis. If the shocks are curved, points in the slit will be illuminated at different apparent times relative to the moving film as the luminous front passes by the slit. Figure 11 presents typical shock profile smears obtained with the pinch tube at the exit of the ring electrode and at a distance of 17.8 centimeters downstream of the pinch discharge for initial tube pressures of 28 and 500 microns of mercury. Since the writing speed of the camera in all cases is slower than the luminous-front velocity, the actual profiles are more curved than indicated on the smears. These pictures show that the shock is roughly parabolic and does not flatten much with distance. The trailing luminosity behind the profile is not uniform and thus indicates that the flow field is not uniform. Reference 22 reports some recent optical interferometer measurements on hydrogen shocks driven by a pinch-tube discharge. The results indicate a very complex flow field and large nonuniformities across the shock tube. The fluctuations in the fringe patterns behind the shock seemed to correspond to the luminosity fluctuations observed in Kerr cell photographs of the shock waves.

Flow duration.- When blunt models were placed in the shock flow, a highly luminous gas cap was formed around the body. The illumination from this gas cap was much more intense than the free-stream radiation. Thus, by filtering out the

free-stream light by a pair of crossed polaroids, a photograph of the bow wave was readily obtained. Figure 12 shows typical examples of the luminous waves about a blunt model and a hollow pipe.

The flow duration was taken as the time a steady standoff distance remained off a blunt model. The buildup of the hot gas on the face of the blunt model was observed with the rotating-mirror camera. For a model position of 75 centimeters from the ring electrode and a pressure of 10 microns of mercury (9μf; 20 kv) a steady luminous standoff distance was found to persist for about 15 microseconds. Ziemer, in reference 6, working with a similar shock tube, found that testing times varied inversely with initial pressure and ranged from 15 to 30 microseconds when the model was about 20 centimeters from the discharge. These flow times would be adequate for certain aerodynamic studies. (See refs. 14 to 16.)

Reflection of shock waves.- In order to get a clearer picture of the nature of the "air" shocks generated by an electrical discharge, the waves were reflected off a plug placed in the shock flow. By examining the nature of these reflected luminous fronts and by comparing the velocities of the oncoming and reflected waves, some additional comments can be made about the shock flow.

A brass plug was placed at positions of 12.7 centimeters, 22.8 centimeters, and 35.6 centimeters from the edge of the ring electrode in the pinch tube. Smear pictures of the reflection process for various initial pressures were obtained through a 1/2-inch slit placed parallel to the tube axis. Figure 13 shows typical smears of the reflection off the plug at 35.6 centimeters for various initial tube pressures. Time increases from right to left. The lines on the streaks are images of distance markers placed 1 inch apart on the shock tube wall. The incident wave travels from the bottom to the top of the smears.

Figure 14 is an enlargement of a typical smear of the propagation of the reflected luminous front near the reflection plug. The smear is divided into three regions of interest. In region A the reflected wave begins to propagate into the oncoming flow at a fairly constant velocity. At about 2 to 3 centimeters from the plug, the front is retarded for roughly 12 microseconds and has almost zero velocity. This is labeled region B. On some of the smears the reflected luminous front was observed to return to the plug wall and reflect again. In region C, the front picks up speed and accelerates into the oncoming flow.

In some ways this description is in qualitative agreement with the hydrodynamic shock model of a reflection process. (See ref. 23.) For example, for strong shocks in a conventional shock tube, the contact surface upon interaction with the reflected wave can act as a fixed boundary. This results in the reflected wave "bouncing" between the reflection wall and contact surface. If this description were also accurate in the case of the observations made from figure 14, the extent of region A would be a measure of the aerodynamic testing time.

The incident and reflected-wave velocities were measured at the reflection plug wall from smears typical of those shown in figure 13. Table I shows the results of these measurements for three plug positions from the ring electrode and for several initial pressures between 30 and 1,000 microns of mercury. For

each case the charging voltage was 20 kilovolts. Also given is the average incident luminous front velocity, that is, the distance of the plug from the ring electrode divided by the time for the luminous front to travel this distance. The theoretical values of the reflected velocity for the measured incident velocity were obtained from reference 24. These results show that the reflected velocities are larger, in general, by a factor of 2 than the theoretical values, which were calculated on the basis of one-dimensional flow in thermal and chemical equilibrium.

This apparent deviation from equilibrium shock theory is in agreement with the experience of other workers with electromagnetic shock tubes. For example, reference 20 reports that the reflection velocities of shock waves generated in these devices from a plane surface are higher than one would calculate on the basis of simple shock theory, and further, that there is no clearly defined interface between the hot gas driver and the shock front. Fowler and Turner (ref. 25), working with a 1-inch magnetically insulated shock tube, found that reflected velocities in hydrogen were greatly increased at some critical axial magnetic-field strength, and they were not able to connect quantitatively the ratio of the reflected to incident waves to an effective specific heat ratio.

The effect of precursor radiation in altering the ambient gas properties has been shown to be important in explaining deviations of the behavior of electromagnetically driven shocks from hydrodynamic theory. McLean and Kolb (ref. 26) reported that discrepancies of approximately a factor of 2 in spectroscopic and hydrodynamic measurements of temperature and density behind strong helium waves generated in a T-tube (ref. 27) could be explained by assuming that ultraviolet radiation from the hot discharge plasma was absorbed by the cold gas ahead of the shock front. Reference 26 also reports that Atkinson, in 1953 (unpublished work), postulated preheating of the cold gas by radiation to explain discrepancies from hydrodynamic theory of measured contact surface and shock velocities in an ohmic heating T-tube (no magnetic driving forces).

Ionization relaxation.- A careful examination of the smears of the reflection process (fig. 13) reveals that the reflected luminosity is seen at the plug wall before the incident luminous front arrives at the plug wall. Color streaks of the reflection process were helpful in explaining these phenomena. They showed that a weak luminous front actually preceded the highly luminous front and that the reflected luminosity began at the point of incidence on the plug of the front of this weakly luminous wave. If it is assumed that the visible radiation of the shock waves is due mainly to processes which involve free electrons, the highly luminous front is taken to be the point at which ionization equilibrium is reached. The extent of the separation of this front and the weakly luminous front would then be a rough measure of the ionization relaxation time in laboratory coordinates.

Niblett and Blackman (ref. 28) have used these phenomena to obtain a lower limit for the ionization relaxation time in air at pressures of 1 to 2 mm of mercury and shock Mach numbers from 11 to 17 (about 0.4 to 0.6 cm/μsec). Their measurements were made in a 1-inch electromagnetic shock tube which was driven by a single-turn induction coil.

Spectra of Discharge From Pinch Tube

Time-average spectra in the visible and near ultraviolet regions were obtained in three different regions of the shock tube with the grating spectrograph. Radiation along the shock tube axis was viewed through an acrylic 1/8-inch-thick window placed at the end of the shock tube. The light was observed by placing the spectrograph slit next to the window without any focusing optics. A mercury discharge tube was used as a calibration source. Spectra were also obtained by looking perpendicular to the tube downstream of the ring electrode and by looking directly at the pinch discharge tube without focusing optics. Samples of the spectra in these three regions are displayed in figure 15.

The spectrum of the radiation viewing up the tube axis (fig. 15) exhibits a background continuum and is characterized by atomic line radiation. There is no evidence of any band structure. In order to obtain spectrum A by viewing perpendicular to the flow and downstream of the discharge, the width of the spectrographic slit had to be increased. Only a few lines can be seen. Spectrum C is similar to spectrum B except that no background continuum is observed and the line intensities are reduced. No lines were observed in spectra A and C that did not appear in spectrum B.

Figure 16 presents an identification of the line radiation observed when viewing up the tube axis as in spectrum B of figure 15. The spectrum was obtained for an initial shock-tube pressure of 10 microns of mercury; the 9μf capacitor bank was charged to 20 kilovolts. In this case a lens was used to place an image of the button electrode at the slit plane of the spectrograph. The wavelengths of the lines were measured from enlargements of the spectrum with a dispersion on the order of 1 A per millimeter; the estimated accuracy of the measurements is about ±0.5 A. References 29 and 30 were used in identifying the radiating atomic species giving rise to the observed spectrum lines. The wavelengths of lines attributed to a specific radiation are designated in figure 16 by the values listed in references 29 and 30. These values are within ±0.5 A of the experimentally measured wave lengths.

The spectrum is characteristic of a spark spectrum in a low-pressure-air discharge. It exhibits a sharp-line series of singly ionized oxygen and a series of singly ionized and neutral nitrogen lines, some of which are hazy and broad. A few argon lines are also identified. Strong silicon lines arising from the glass wall contamination and some weak copper lines are observed. The suppression of copper radiation is strange in view of the fact that the electrodes did show some surface conditioning and erosion. In contrast to this low-pressure spectrum, the radiation from the atmospheric-air-gap switch discharge showed only copper lines and contamination lines from the brass trigger. No lines characteristic of "air" radiation were observed and there was no background continuum.

The lines identified as the persistent lines of Ca II at 3933.67 and 3968.47, and of Al I at 3944.03 and 3961.53 are open to some question. They appeared in all spectra obtained including that of the air-gap switch discharge. The air-spark spectrum line list in reference 29 includes observed lines at 3933.6 A and 3968.4 A and identifies them with a question mark. An argon line does lie at 3968.36 A, but the strength of the observed line compared with the other lines identified as argon lines in figure 16 would tend to preclude this possibility.

It would appear that, within the experimental accuracy, the Ca II lines are present. In the case of the lines at 3944.0 A and 3961.5 A, the conclusion that they are Al I lines was drawn on the basis that none of the other species known to be present had any lines, with the exception of an argon line at 3944.27 A, within ±0.5 A of the Al I lines. The possibility of the argon line was rejected since the 3944.0 A line appeared in the air-gap discharge spectrum in which the suppression of "air" radiation was complete. The origin of the lines attributed to calcium and aluminum is not certain.

The hydrogen β line at 4861.3 A is believed to be observed in figure 16 and is attributed to water vapor in the air. The line is considerably broadened and quite nebulous.

Reference 4 also presents time-integrated spectra of the radiation from an electromagnetic shock tube operated in air. The results were in qualitative agreement with the observations made here.

Modifications of the Electromagnetic Shock Tube

One of the major drawbacks of the ringing electric discharge in generating strong shocks is that the resulting flow is made up of a series of interacting luminous waves which eventually settle into a single but nonuniform wave downstream of the discharge. The ringing of the discharge and the resulting multiple waves could be prevented by using ignitron switches to permit a single energy pulse to be delivered to the gas. However, because of the rapid attenuation of a single luminous front, much higher energy supplies would be required to maintain strong shocks downstream of the discharge in heavy gases such as air.

A more fruitful modification of the electromagnetic shock tube, where aerodynamic studies in heavy gases are the objective, is to employ very light diaphragms (on the order of several thousands of a millimeter thick) just downstream of the discharge at about two or three tube diameters. This would allow different gases to be used in the discharge and expansion sections and would allow exploration of more direct analogies to the piston-driven shock wave. With the employment of diaphragms the ringing of the discharge might not be undesirable as the interactions of multiple waves prior to striking the diaphragm would result in a higher energy driving condition after bursting. Some attempt might be made to force mixing of these first waves before reaching the diaphragm to establish a more uniform driver gas condition. A recent investigation (ref. 31) successfully used diaphragms in a T-tube generator and demonstrated that a contact surface existed between the driver and driven gases for combinations of hydrogen and argon gases.

Variations in the geometry of the expansion tube at the exit of the shock generator would also be useful in improving the shock flow. For example, it was demonstrated in reference 18 that, in the case of a conical generator, radial expansion of the pinched gas as it exits from the discharge region could be prevented by means of abrupt reduction of the size of the exit channel diameter or by funneling of the exit shocks into the expansion tube. By restricting the exit area of the discharge gas, more energetic shocks with longer gas drivers were obtained in deuterium.

Application of the Shock Flow to Aerodynamic Problems

The aerodynamic capabilities of devices similar to the one described in this paper have not been fully explored. With the exception of Ziemer's work (ref. 6) little has been done in applying the electromagnetic shock tube to aerodynamic reentry studies. This is due in part to the complexity of the flow which is generated by the spark discharge (a recent preliminary interferometric study of electromagnetic shocks (ref. 22) clearly points out the nonuniform density profiles exhibited by these waves), and to the failure of the usual shock theory to explain the mechanism of the wave propagation. The high degree of ionization behind the shocks and the appearance of precursor radiation (see refs. 20, 26, and 27), which alters the properties of the unshocked gas, require special theoretical treatments. To date, no completely satisfactory model has been proposed to account adequately for the various anomalies occurring in the case of electromagnetically driven shock waves. References 32, 33, and 34 give evidence that a "hot electron gas" is responsible for driving the luminous waves in conical and T-tube drivers and that the ionic temperature behind the shocks is very low. On the other hand, reference 35 explains the action of an electromagnetic shock tube, having an electrode geometry similar to the button-ring configuration discussed in this report, by means of a magnetic driver principle in which the kinetic energy of the gas is small compared with the magnetic energy imbedded in the gas. In addition to these investigations it has been shown in reference 31 that at sufficient diameters from the spark discharge region (about 9 tube diameters) in a T-tube the origin of the luminous front is in shock heating at the wave front and is not tied to excitation in the discharge region. Thus, at sufficient distances from the spark discharge one could perform relaxation studies in shock heating with some validity, for example, as in reference 28. However, the effect of precursor radiation as well as of electrode and wall contamination in altering the shock flow must still be considered as limitations on such studies.

These complex characteristics of electromagnetically driven waves severely limit its capability as an aerodynamic facility. However, some qualitative studies of the effects of the hot ionized gas cap formed around blunt objects placed in the shock flow might be performed when the conductivity of the gas is the most important parameter to be considered. For example, the problem of radio attenuation through the gas cap could be measured as a function of the degree of ionization or conductivity of the hot plasma bow wave. On the other hand, the problem of radiant heat transfer from the bow wave to the model would depend strongly on a knowledge of the gas composition and degree of deviation from equilibrium conditions. It would not appear that the electromagnetic shock tube could be used with confidence for controlled radiant heat-transfer studies.

CONCLUDING REMARKS

An evaluation study of an electromagnetic shock tube was undertaken to determine the suitability of the shock flow for aerodynamic studies at supersatellite velocities. Smear pictures of the propagating luminous fronts generated by a high-voltage spark discharge showed that velocities between 2 to 4 cm/μsec were obtained

at distances of 2 tube diameters from the discharge region. At about 8 tube diameters these velocities decayed to less than 1 cm/μsec. Multiple shocks were generated by the ringing of the discharge and these interacted with the primary wave downstream. The luminous fronts were observed to have parabolic-like contours, and the lumination patterns behind these fronts were nonuniform suggesting irregularities in the flow and nonequilibrium temperatures.

The reflection of these luminous waves in a pinch-tube shock generator gave reflected velocities which were larger by about a factor of 2 than expected on the basis of equilibrium hydrodynamic theory (no field effects). Although the behavior of the reflected wave upon interaction with the oncoming shock flow exhibited characteristics which were qualitatively similar to that predicted by hydrodynamic shock theory, the observations were insufficient to establish the existence of a contact surface for these electromagnetically generated shocks.

Steady bow wave standoff distances in front of a blunt model in the flow were on the order of 10 microseconds. If this has been interpreted as the duration of steady flow for purposes of aerodynamic testing, these flow times would be adequate for certain aerodynamic studies.

Time-integrated spectra of the discharge were found to be characteristic of a low pressure spark in air as anticipated.

It was concluded that, because of the complex flow characteristics observed in the electromagnetic shock tube, aerodynamic studies, and in particular radiation heat-transfer studies, could not be performed in this device with confidence.

Langley Research Center,
National Aeronautics and Space Administration,
Langley Station, Hampton, Va., June 11, 1963.

REFERENCES

1. Fowler, Robert J., and Lee, Richard G.: Rayleigh Afterglow in Hydrogen Discharges. Phy. Rev. (Letters to the Editor), vol. 81, no. 3, Feb. 1, 1951, pp. 457-458.

2. Fowler, Richard G., Goldstein, Jack S., and Clotfelter, Beryl E.: Luminous Fronts in Pulsed Gas Discharges. Phy. Rev., vol. 82, no. 6, June 15, 1951, pp. 879-882.

3. Kolb, A. C.: Experiments at U.S. Naval Research Laboratory. Magnetohydrodynamics, Rolf K. M. Landshoff, ed., Stanford Univ. Press (Stanford, Calif.), c.1957.

4. Kash, S. W.: Experiments at Lockheed Missile Systems Division. Magnetohydrodynamics, Rolf K. M. Landshoff, ed., Stanford Univ. Press (Stanford, Calif.), c.1957.

5. Josephson, Vernal: Production of High-Velocity Shocks. Jour. Appl. Phys., vol. 29, no. 1, Jan. 1958, pp. 30-32.

6. Ziemer, Richard W.: Electromagnetic Shock Tubes. Dynamics of Conducting Gases. Proc. Third Biennial Gas Dynamics Symposium, Ali Bulent Cambel, and John B. Fenn, eds., Northwestern Univ. Press, c.1960.

7. Barger, R. L., Brooks, J. D., and Beasley, W. D.: The Design and Operation of a Continuous-Flow Electrodeless Plasma Accelerator. NASA TN D-1004, 1962.

8. Barger, R. L., Brooks, J. D., and Beasley, W. D.: An Experimental Study of Continuous Plasma Flows Driven by a Confined Arc in a Transverse Magnetic Field. NASA TN D-716, 1961.

9. Wood, George P., and Carter, Arlen F.: Considerations in the Design of a Steady DC Plasma Accelerator. [Preprint] 903-59, American Rocket Soc., Aug. 1959.

10. Wood, George P., Carter, Arlen F., Sabol, Alexander P., and Weinstein, Richard H.: Experiments in Steady State Crossed-Field Acceleration of Plasma. The Physics of Fluids (Letters to the Editor), vol. 4, no. 5, May 1961, pp. 652-653.

11. Hess, Robert V.: Experiments and Theory for Continuous Steady Acceleration of Low Density Plasmas. Vol. I of Proc. XIth Int. Astronautical Cong., Carl W. P. Reuterswärd, ed., Springer-Verlag (Vienna), 1961, pp. 404-411.

12. Matthews, Clarence W., and Cuddihy, William F.: Experimental Study of a Single-Coil Induced-Electromotive-Force Plasma Accelerator. NASA TN D-639, 1961.

13. Turner, Eugene B., and Eastmond, E. John: Conductivity Measurement of Deuterium Plasmas at Magnetic Reynolds Numbers Greater Than Unity. GM-TR-0165-00514 (Contract AF 04(647)-165), Space Tech. Labs., Dec. 4, 1958.

14. Ziemer, Richard W.: Experimental Investigation in Magneto-Aerodynamics. ARS Jour., vol. 29, no. 9, Sept. 1959, pp. 642-647.

15. Ziemer, Richard W.: Effects of a Magnetic Field on the Hypervelocity Flow About a Blunt Body. GM-TR-0165-00464 (Contract No. AF 04(647)-165), Space Tech. Labs., The Ramo-Wooldridge Corp., Aug. 27, 1958.

16. Phillips, William R., and Valade, Larry G.: Design of an Infrared System for Measuring Stagnation Point Heat Transfer Rates in an Electromagnetic Shock Tube. M. S. Thesis, U.S. Naval Postgraduate School, 1959.

17. Ziemer, Richard W.: Instrumentation for Magnetoaerodynamic Heat Transfer. STL/TR-60-0000-09290 (Contract No. AF 04(647)-309), Space Tech. Labs., Inc., Sept. 8, 1960.

18. Josephson, Vernal, and Hales, Richard W.: Parametric Study of the Conical Shock Tube. The Physics of Fluids, vol. 4, no. 3, Mar. 1961, pp. 373-379.

19. Cobine, James Dillon: Gaseous Conductors. Dover Pub., Inc., c.1958.

20. Josephson, Vernal, and Hales, Richard W.: The Structure of an Electromagnetically Driven Shock Tube. STL/TR-60-0000-19313 (Contract No. AF 04(647)-309), Space Tech. Labs., Inc., Sept. 15, 1960.

21. Harris, E. G.: Exact and Approximate Treatments of the One-Dimensional Blast Wave. Rep. No. 4858, U.S. Naval Res. Lab., Nov. 23, 1956.

22. Klein, Alan F.: Some Results Using Optical Interferometry for Plasma Diagnostics. The Physics of Fluids (Res. Notes), vol. 6, no. 2, Feb. 1963, pp. 310-311.

23. Glass, I. I., and Hall, J. Gordon: Handbook of Supersonic Aerodynamics. Section 18 - Shock Tubes. Navord Rep. 1488 (Vol. 6), Dec. 1959.

24. Ziemer, Richard W.: Extended Hypervelocity Gas Dynamic Charts for Equilibrium Air. STL/TR-60-0000-09093 (Contract No. AF 04(647)-309), Space Tech. Labs., Inc., Apr. 14, 1960.

25. Fowler, Richard G., and Turner, Eugene B.: A Magnetically Insulated Shock Tube. STL/TR-60-0000-09180 (Contract No. AF 04(647)-309), Space Tech. Labs., Inc., June 1960.

26. McLean, E. A., Kolb, A. C., and Griem, H. R.: Visible Precursor Radiation in an Electromagnetic Shock Tube. The Physics of Fluids, vol. 4, no. 8, Aug. 1961, pp. 1055-1056.

27. McLean, E. A., Faneuff, C. E., Kolb, A. C., and Griem, H. R.: Spectroscopic Study of Helium Plasmas Produced by Magnetically Driven Shock Waves. The Physics of Fluids, vol. 3, no. 6, Nov.-Dec. 1960. pp. 843-856.

28. Niblett, Bryan, and Blackman, Vernon H.: An Approximate Measurement of the Ionization Time Behind Shock Waves in Air. Jour. Fluid Mech., vol. 4, pt. 2, June 1958, pp. 191-194.

29. Harrison, George R., compiler: Massachusetts Institute of Technology Wavelength Tables. John Wiley & Sons, Inc., 1960.

30. Hodgman, Charles D., Weast, Robert C., and Selby, Samuel M., eds.: Handbook of Chemistry and Physics. Forty-first ed., Chemical Rubber Pub. Co., 1959-1960.

31. Edwards, B. D.: Confirmation of the Origin of the Luminosity Behind the Shock Wave in an Electromagnetically Driven Shock Tube. Nature, vol. 196, no. 4857, Dec. 1, 1962, pp. 833-835.

32. Fowler, R. G., and Fried, B. D.: Theory of Electron Driven Shock Waves. STL/TR-60-0000-GR310, Space Tech. Labs., Inc., Sept. 16, 1960.

33. Fowler, R. G., Paxton, G. W., and Hughes, H. G.: Electrons as a Shock Driver Gas. Physics of Fluids, vol. 4, no. 2, Feb. 1961, pp. 234-237.

34. Fowler, Richard G.: Origin of the Driving Force in Electromagnetic Shock Tubes. The Physics of Fluids, vol. 6, no. 4, Apr. 1963, pp. 548-549.

35. Pugh, Evan R.: Studies of the Phenomena Occurring in an Electromagnetic Shock Tube. Contract No. Nonr-401(25), Graduate School of Aero. Eng., Cornell Univ., 1962.

TABLE I.- COMPARISON OF MEASURED REFLECTED LUMINOUS FRONT VELOCITY TO THE PREDICTED REFLECTED-SHOCK VELOCITY BASED ON EQUILIBRIUM, ONE-DIMENSIONAL SHOCK TUBE BEHAVIOR

Distance of plug from ring electrode, x, cm	Initial shock-tube pressure, p_1, μHg	Average shock velocity, $U_{s,av}$, cm/μsec	Measured incident-shock velocity at plug, $U_{s,ex}$, cm/μsec	Measured reflected-shock velocity at plug, $U_{r,ex}$, cm/μsec	Theoretical equilibrium reflected-shock velocity, $U_{r,theor.}$, cm/μsec
12.7	31	1.46	1.23	0.27	0.16
	50	2.96	1.79	.25	----
	350	1.79	.91	.33	.13
	500	1.71	.98	.21	.14
	1,000	.96	.64	.20	.09
22.9	31	1.18	.92	.25	.11
	46	1.44	1.06	.20	.13
	70	1.70	1.19	.15	.16
	125	1.18	1.06	.30	.14
	300	1.22	.82	.15	.12
	510	.94	.69	.30	.10
	1,000	.64	.53	.27	.08
35.6	34	.69	.63	.17	.08
	59	.84	.60	.25	.07
	130	.86	.62	.13	.08
	255	.78	.63	.15	.09
	500	.72	.62	.20	.09
	1,000	.57	.47	.24	.07

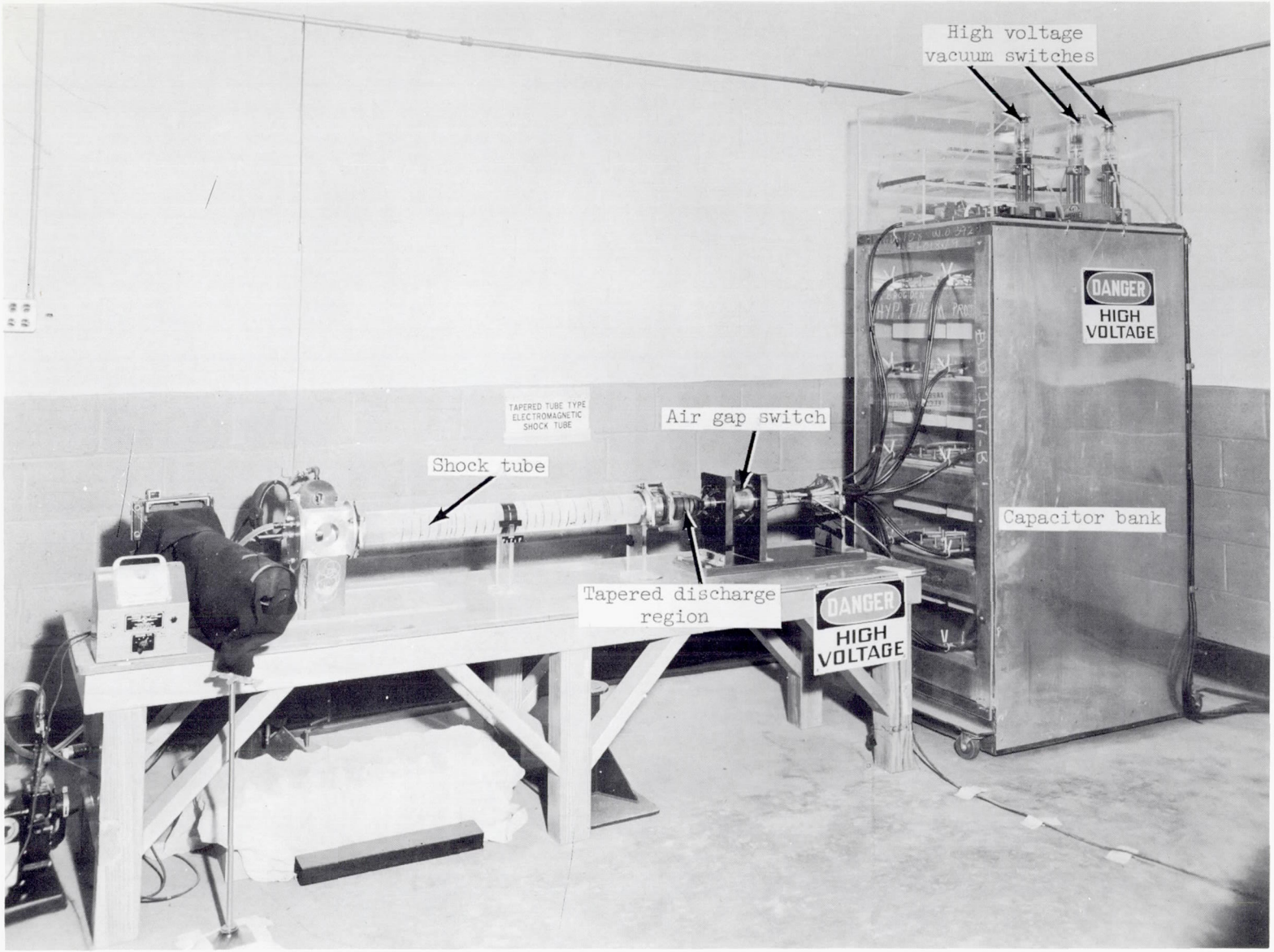

Figure 1.- Photograph of the electromagnetic shock tube. L-62-5913.1

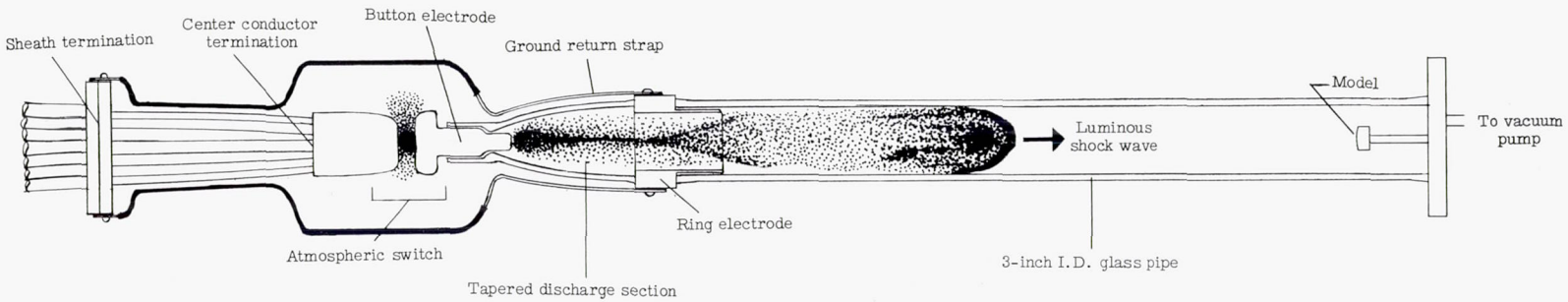

Figure 2.- Sketch of electromagnetic shock tube with pinch-tube electrode configuration.

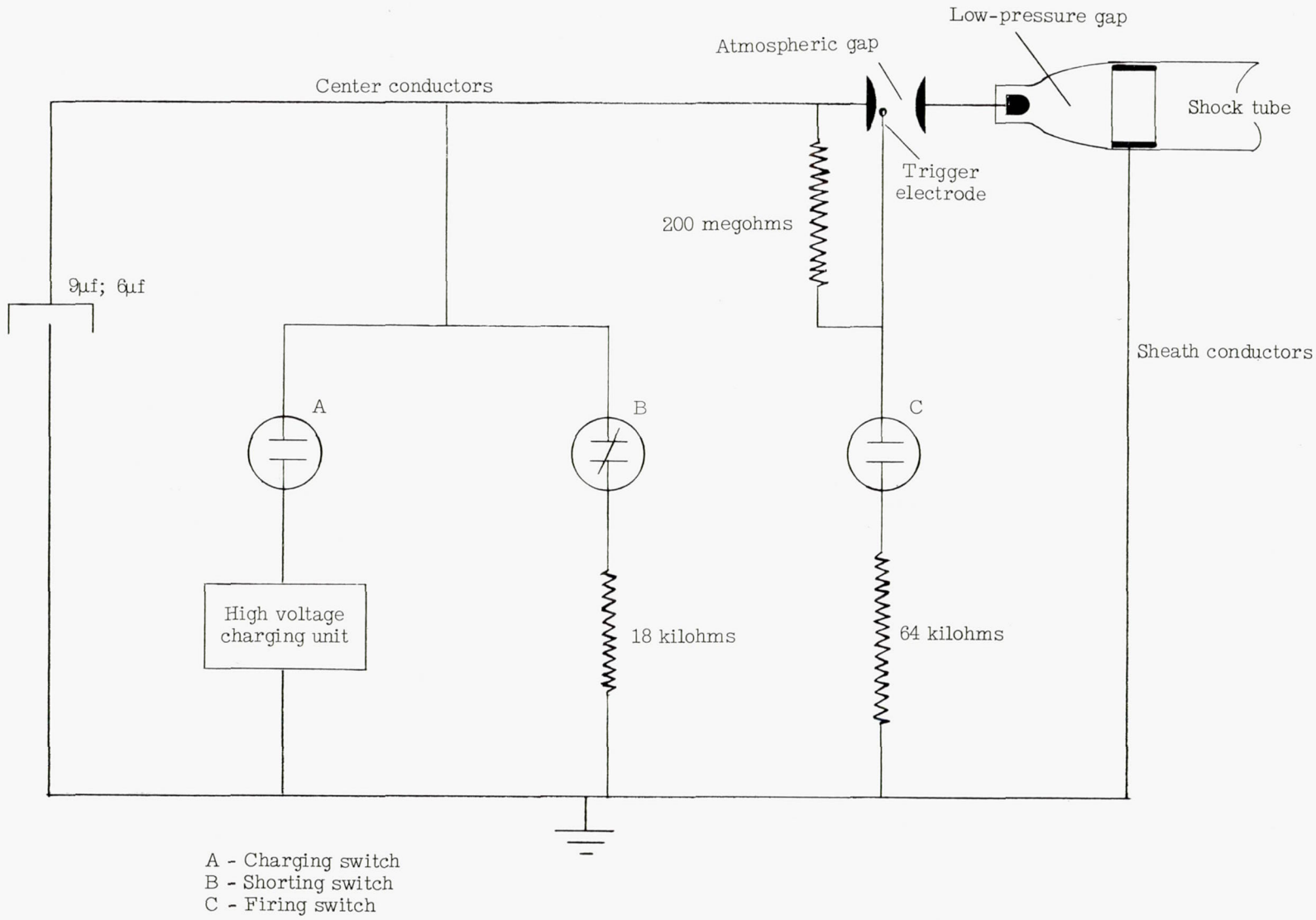

Figure 3.- Circuit diagram of shock generator.

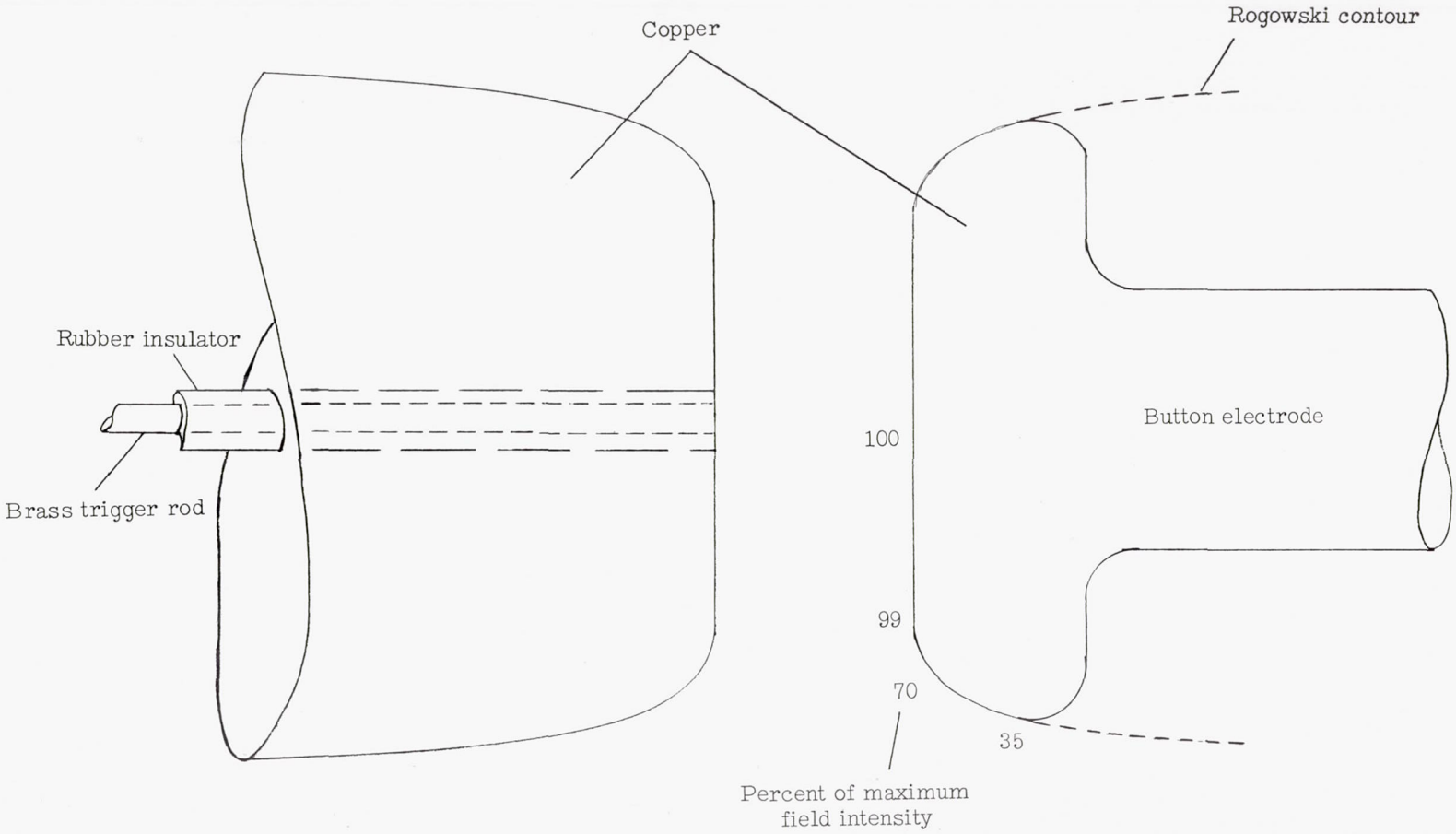

Figure 4.- Sketch of atmospheric-air-gap switch.

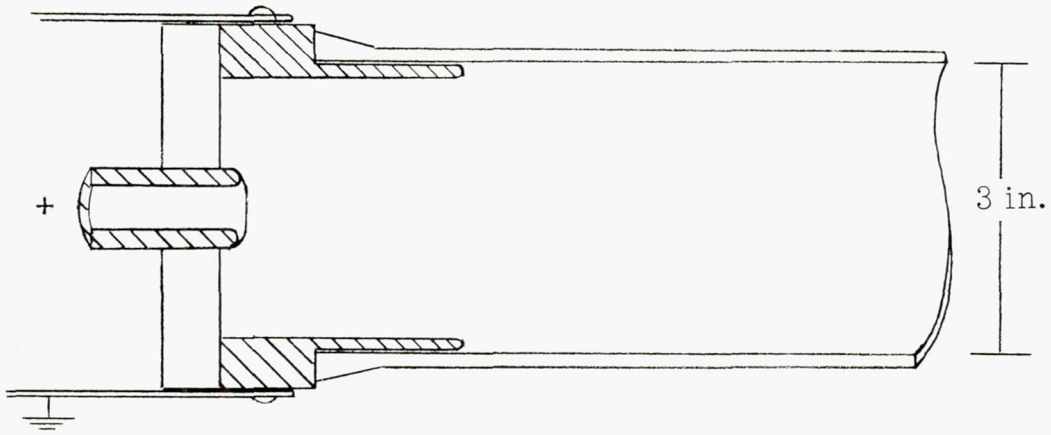

(a) Hollow button ring.

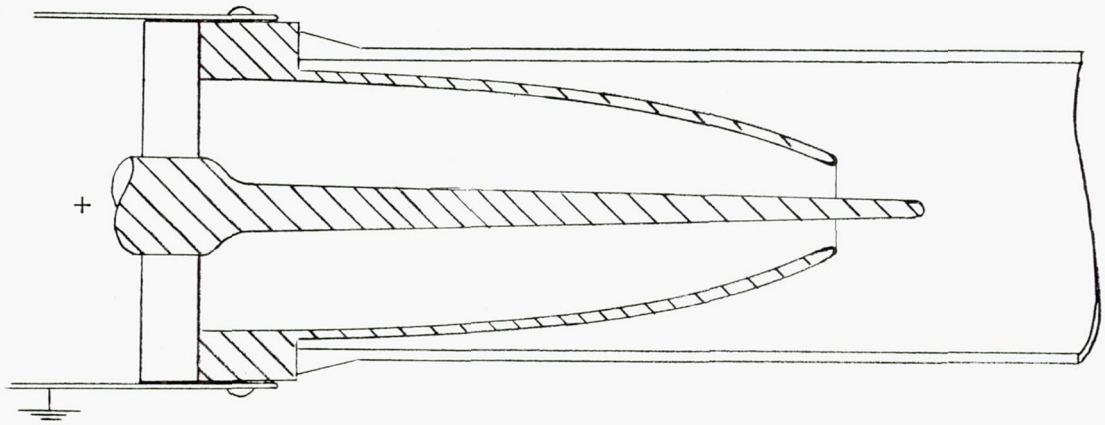

(b) Aluminum spindle cone.

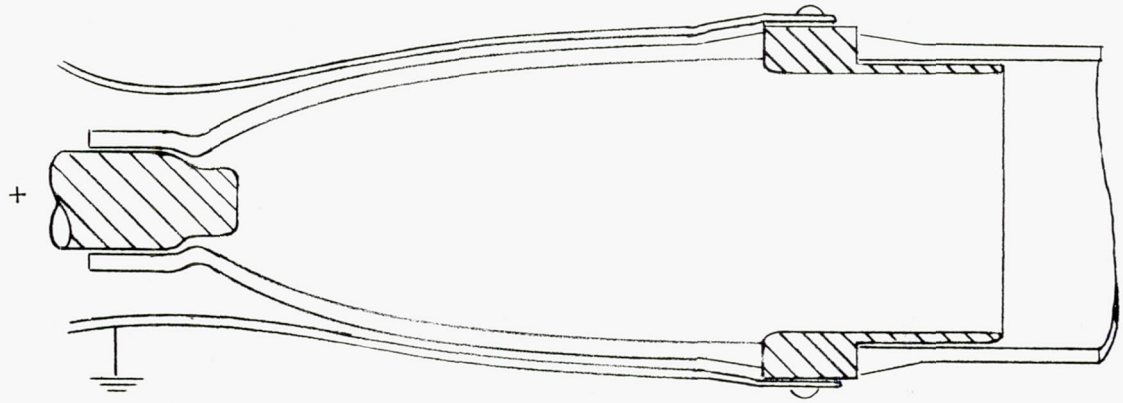

(c) Pinch tube.

Figure 5.- Sketch of electrode configurations.

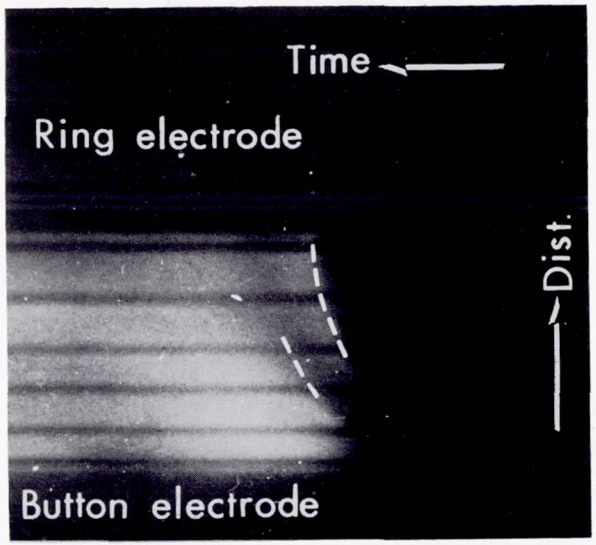

(a) Velocity smear.

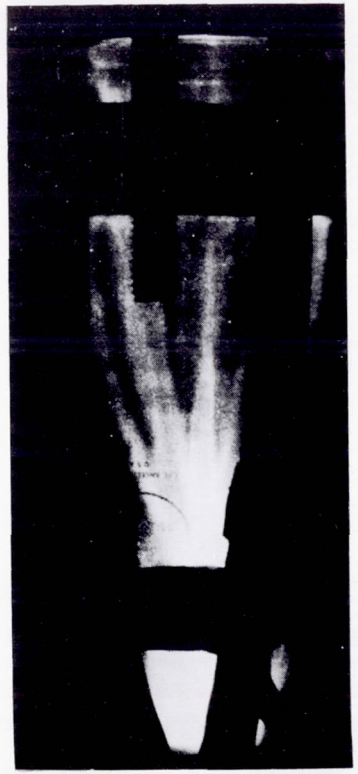

(b) One-tenth μsec Kerr cell exposure.

L-63-3185

(c) Time-average photograph.

Figure 6.- Characteristics of the discharge in the pinch-tube shock generator.

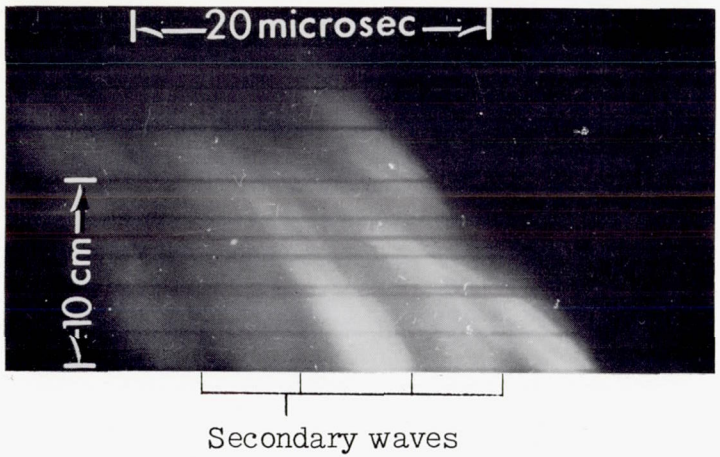

(a) Button-ring generator (17.5 kv; 6μf).

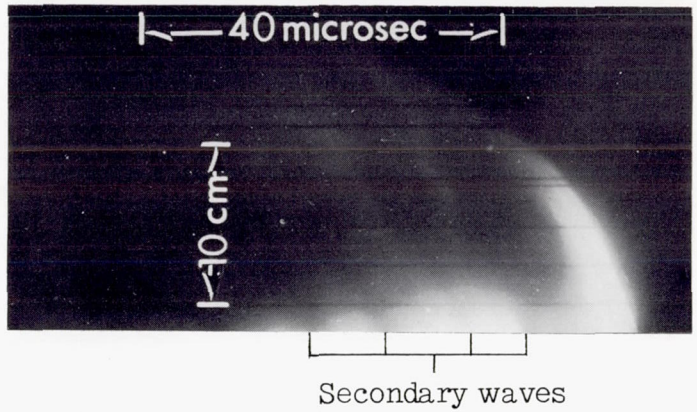

(b) Spindle-cone generator (15 kv; 6μf).

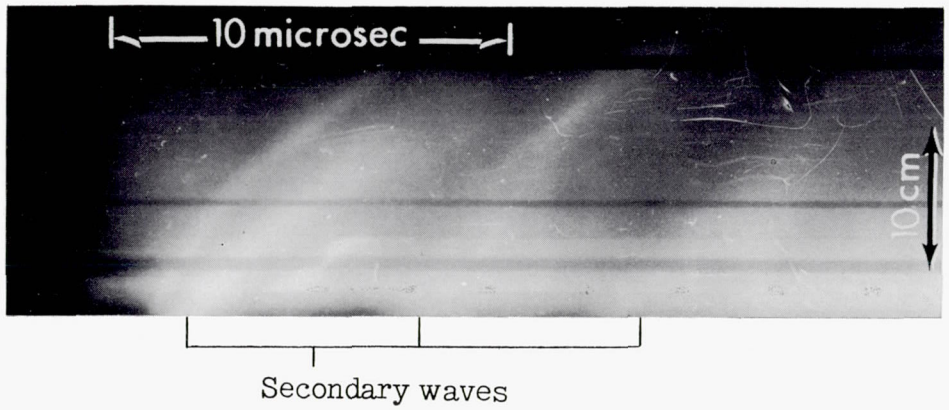

(c) Pinch-tube generator (20 kv; 9μf). L-63-3186

Figure 7.- Typical smear camera photographs of the luminous shock front propagation.

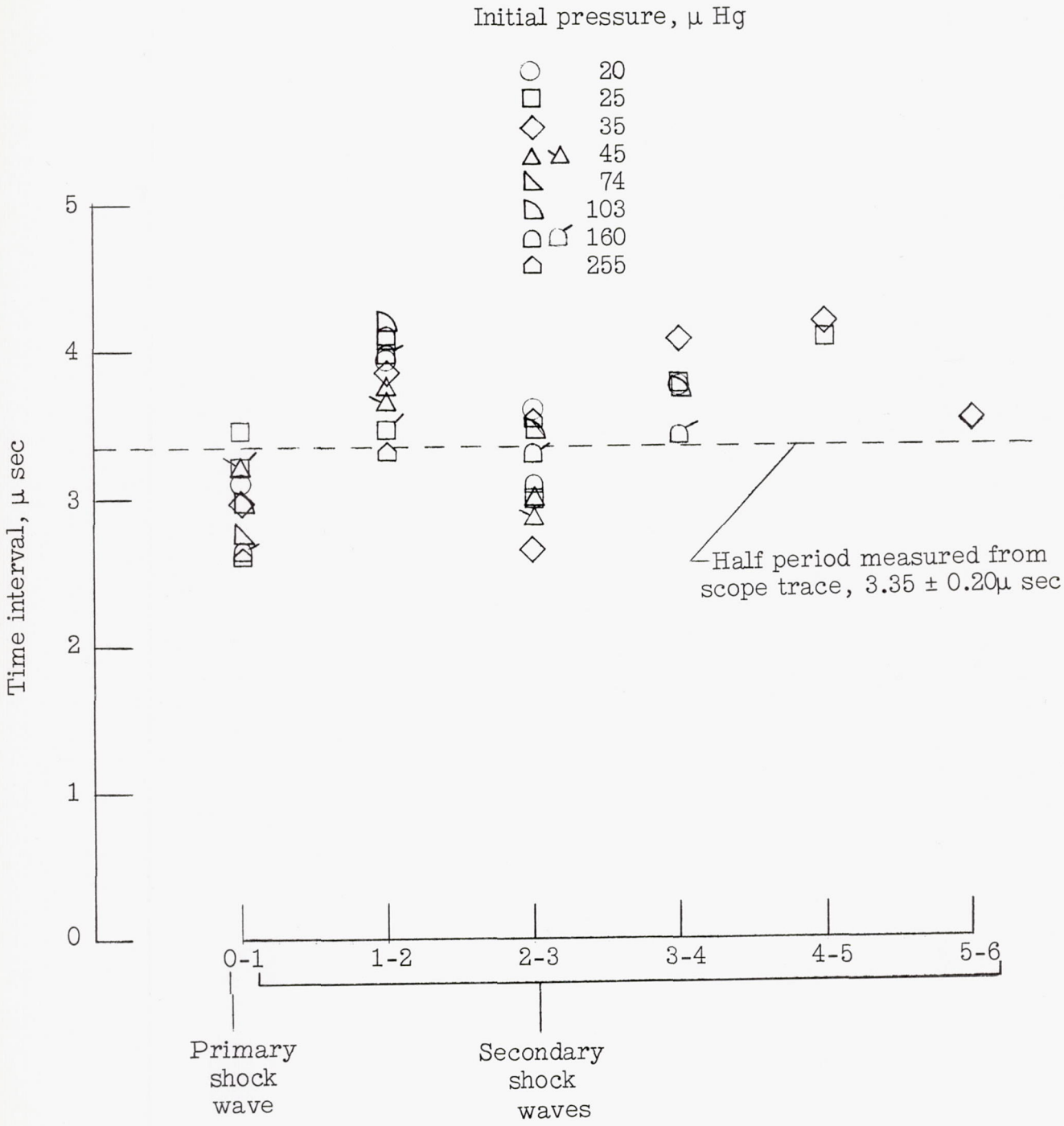

Figure 8.- Time interval between the appearance of successive shocks at a station 15.2 cm from the edge of the ring electrode for the button-ring configuration at 17.5 kv and 6μf.

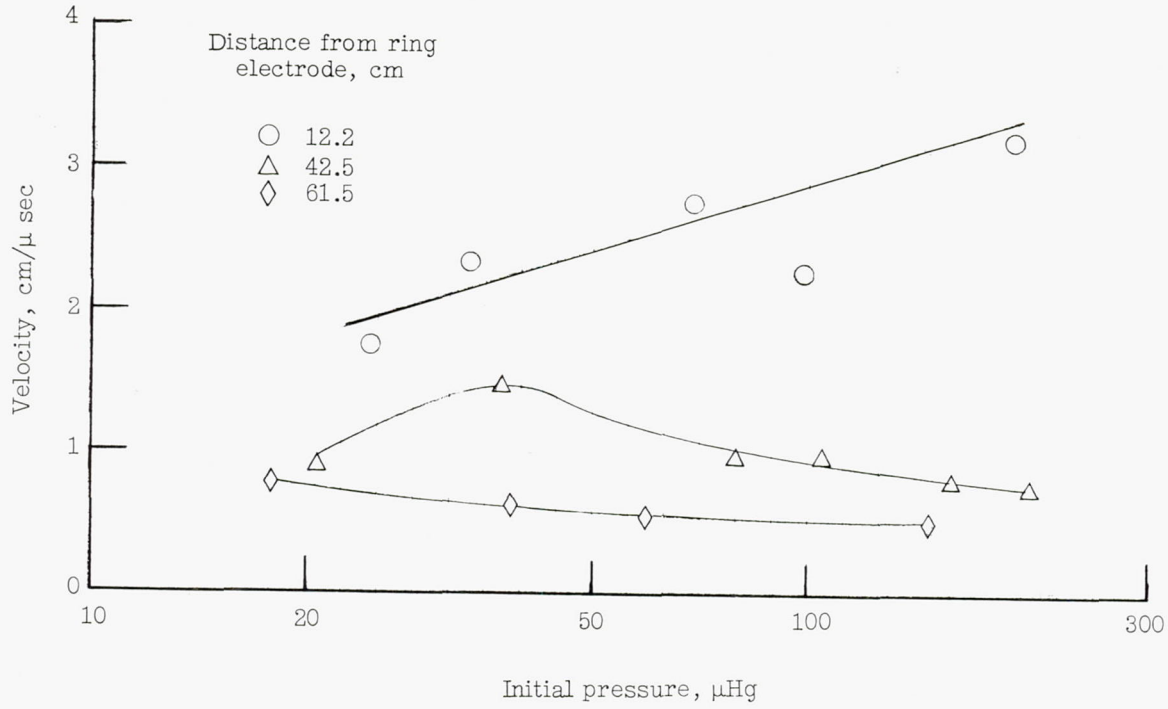

(a) Button-ring configuration (12.5 kv; 6μf).

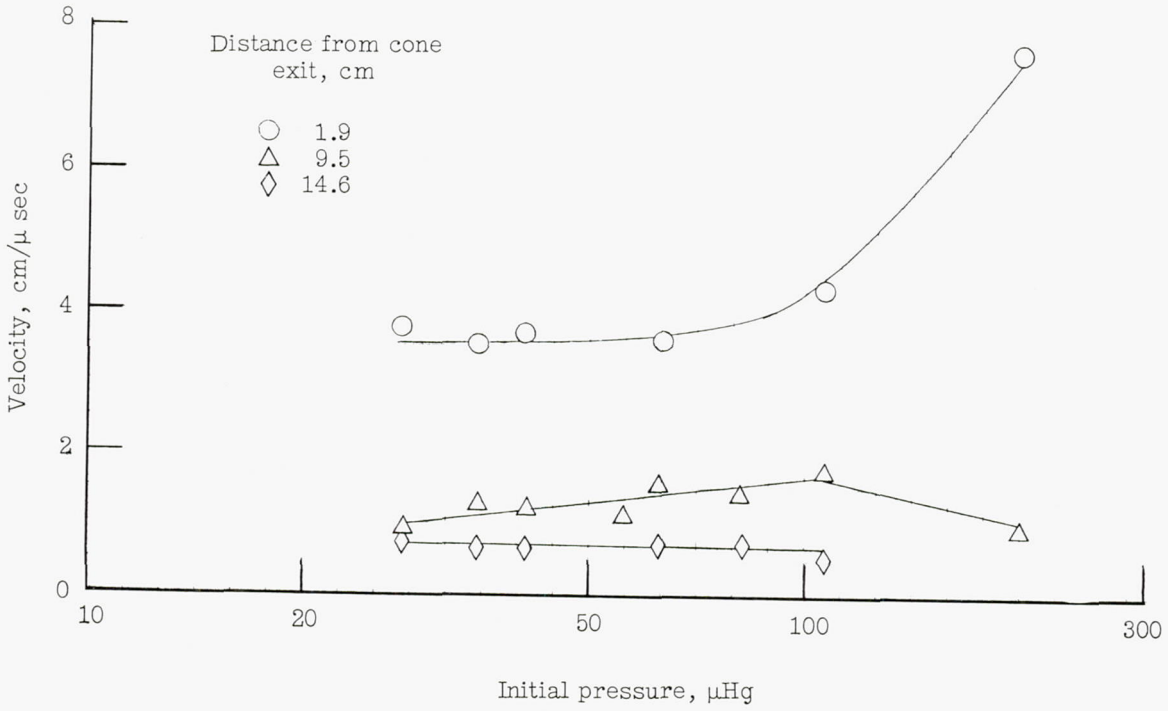

(b) Spindle-cone configuration (15 kv; 6μf).

Figure 9.- Luminous front velocity as a function of initial tube pressure and distance from shock generator.

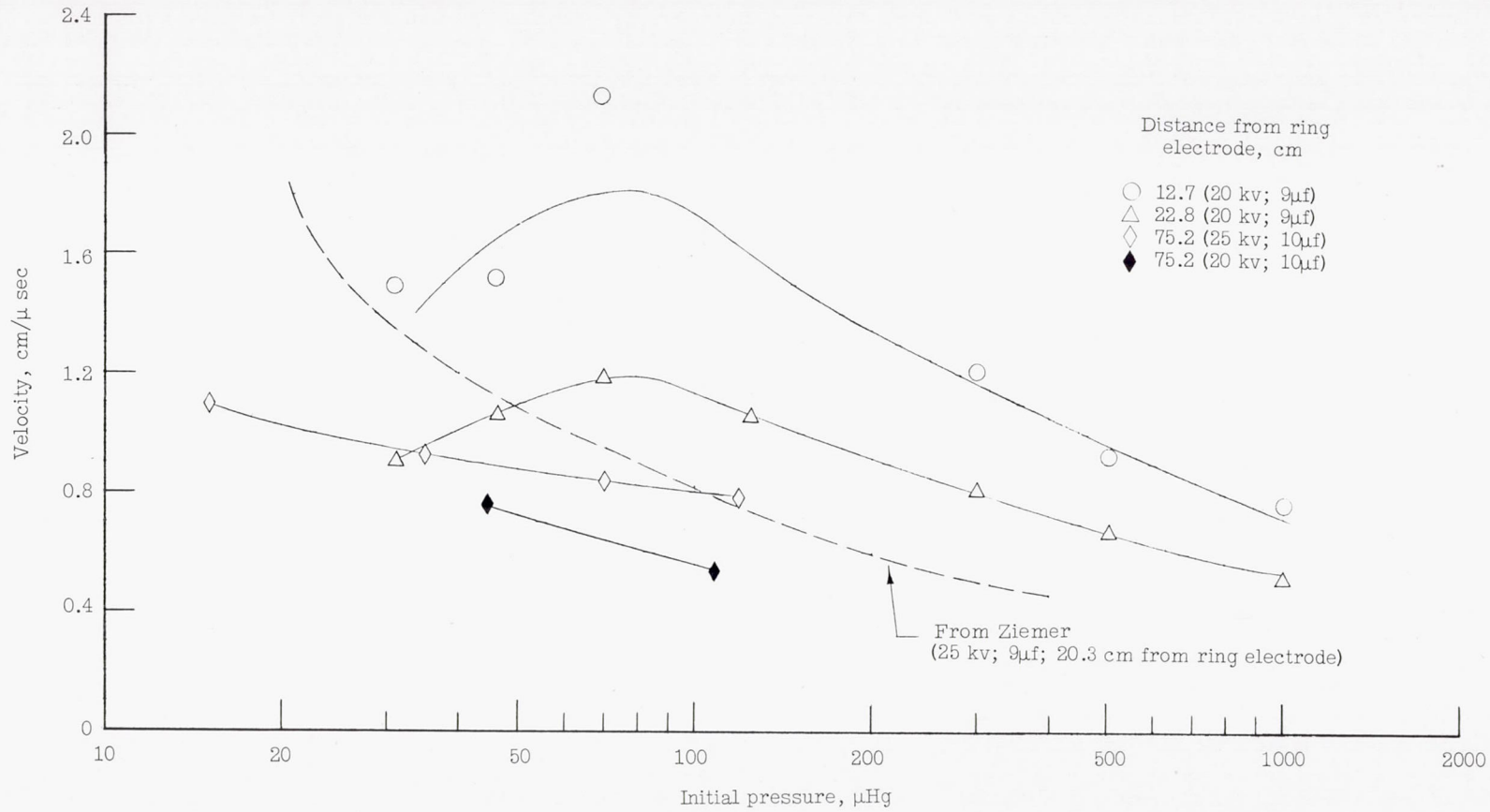

(c) Pinch-tube configuration.

Figure 9.- Concluded.

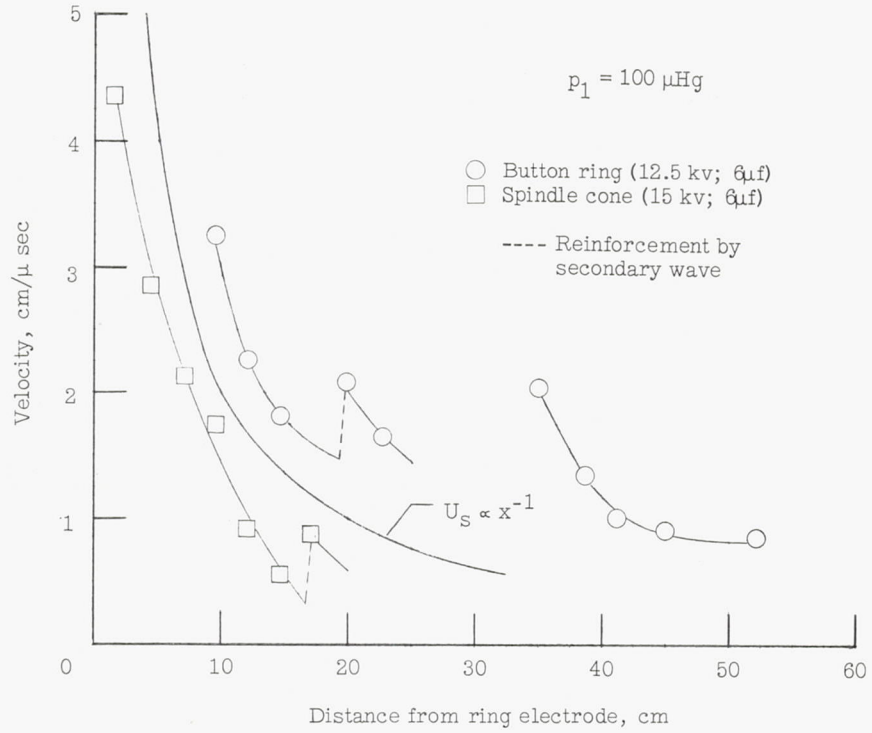

(a) Button-ring and spindle-cone configurations.

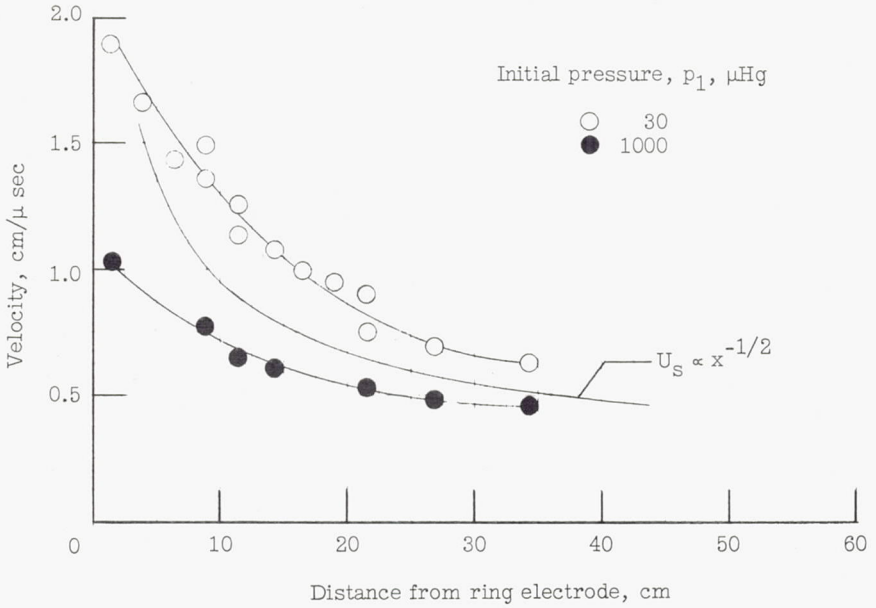

(b) Pinch-tube configuration (20 kv; 9μf).

Figure 10.- Plots illustrating the luminous front velocity decay at the exit of the shock generators.

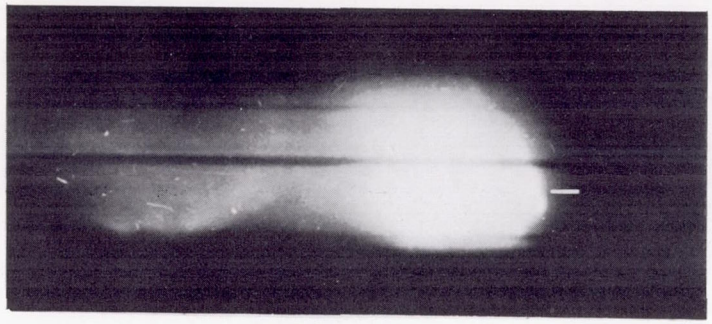

28μHg

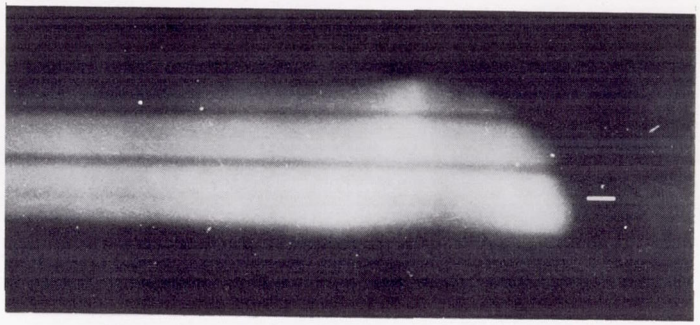

28μHg

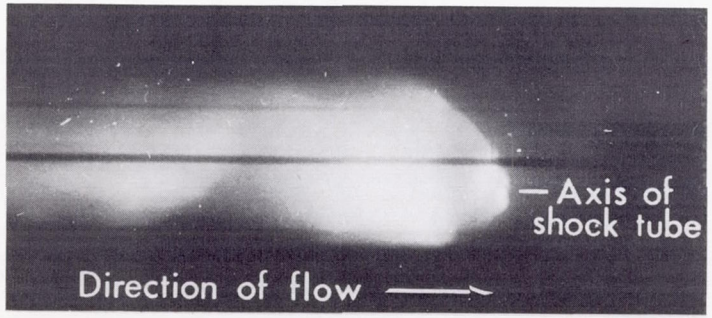

500μHg

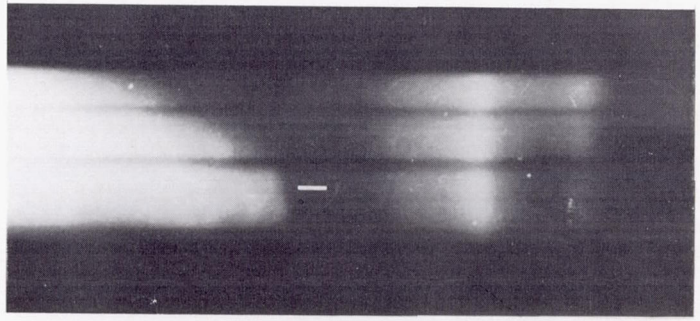

500μHg

L-63-3187

(a) At exit of ring electrode.

(b) At 17.8 centimeters from ring electrode.

Figure 11.- Profile of shocks generated by pinch-tube discharge at 20 kv; 9μf.

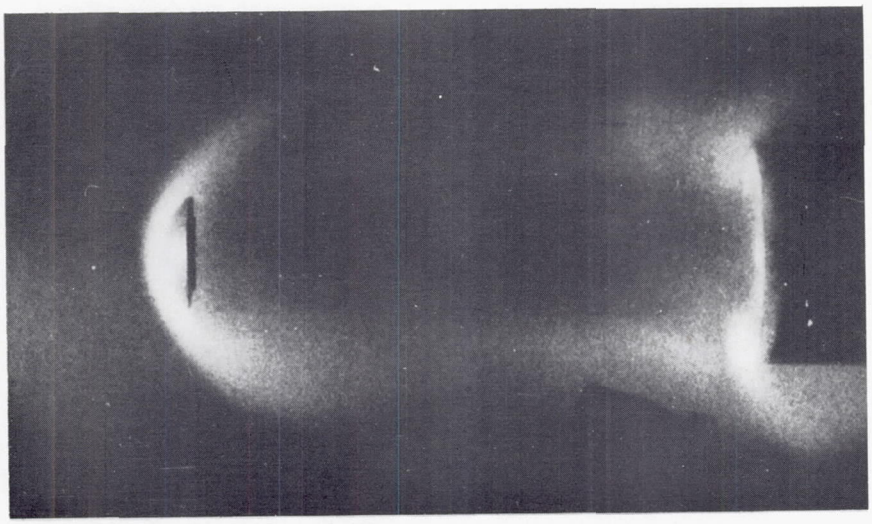

Model: bolt head

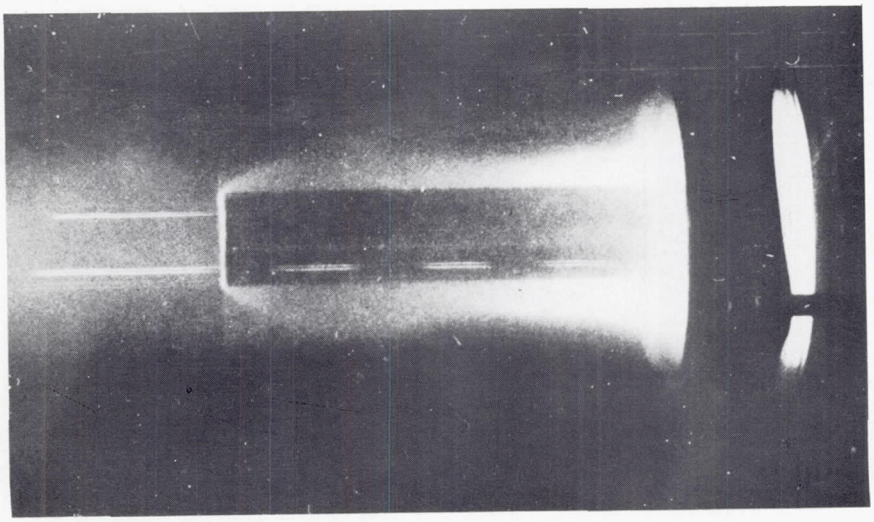

Model: hollow steel pipe

L-63-3188

Figure 12.- Time-average photographs of luminous gas caps around objects in the shock flow.

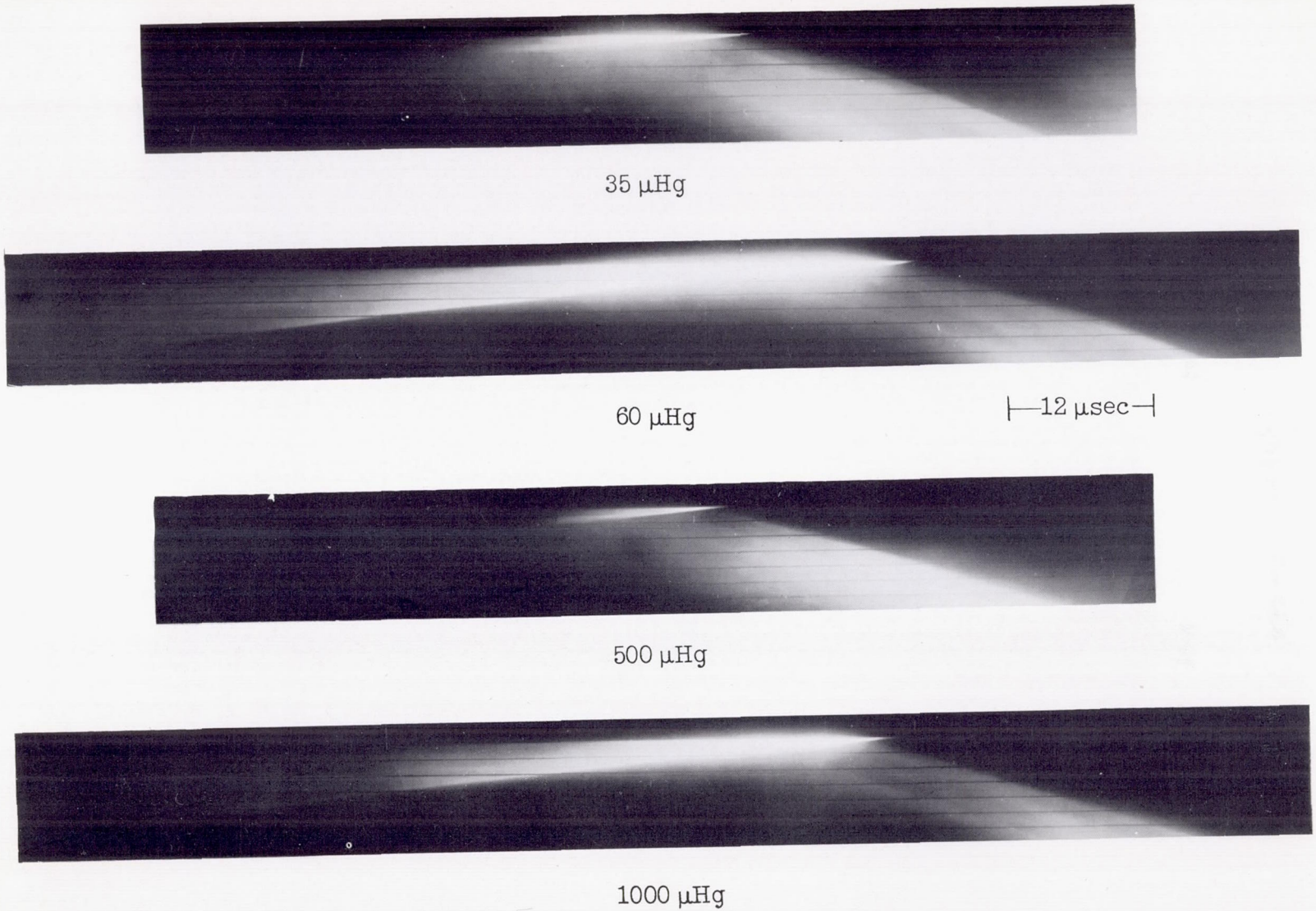

L-63-3189

Figure 13.- Velocity smears of reflection off plug at a distance of 35.6 centimeters from the ring electrode in the pinch-tube discharge (20 kv; 9μf).

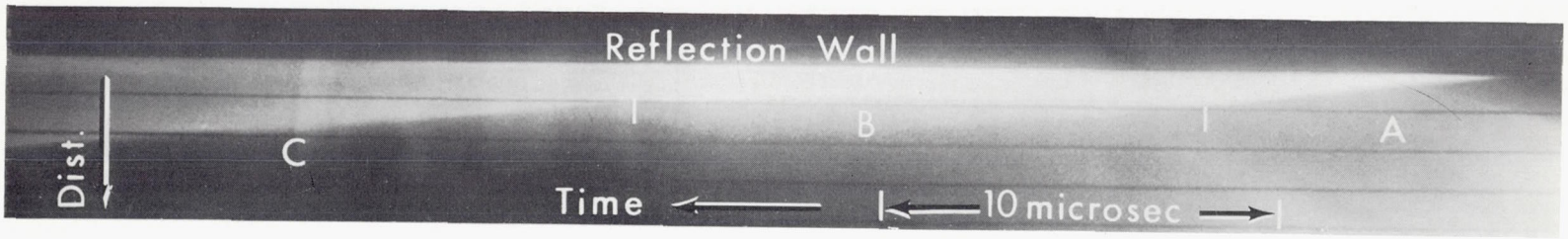

Region A - Initial reflected wave
Region B - Interaction with on-coming flow
Region C - Increasing reflected shock velocity

Figure 14.- Typical velocity smear showing details of the reflection process. L-63-3190

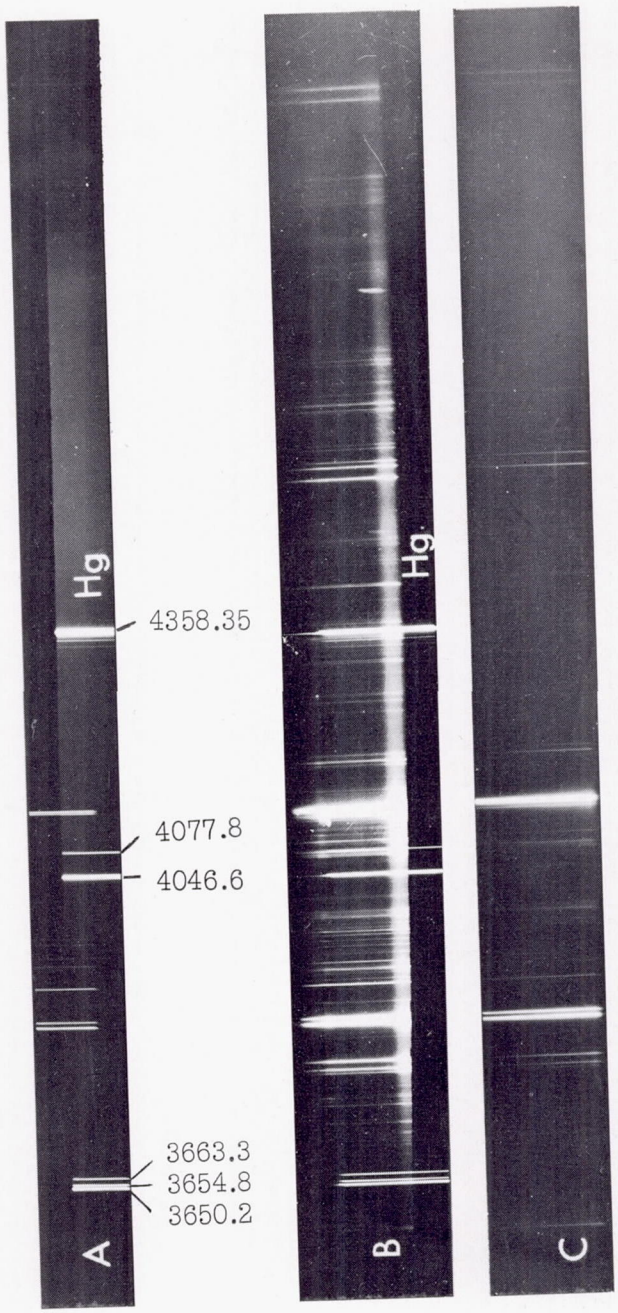

A - Viewing perpendicular to flow downstream of ring electrode
B - Viewing up the shock tube axis
C - Viewing perpendicular to tapered discharge region

L-63-3191

Figure 15.- Time-average spectra of radiation from shock-tube discharge (pinch-tube configuration at 20 kv; 10 μHg).

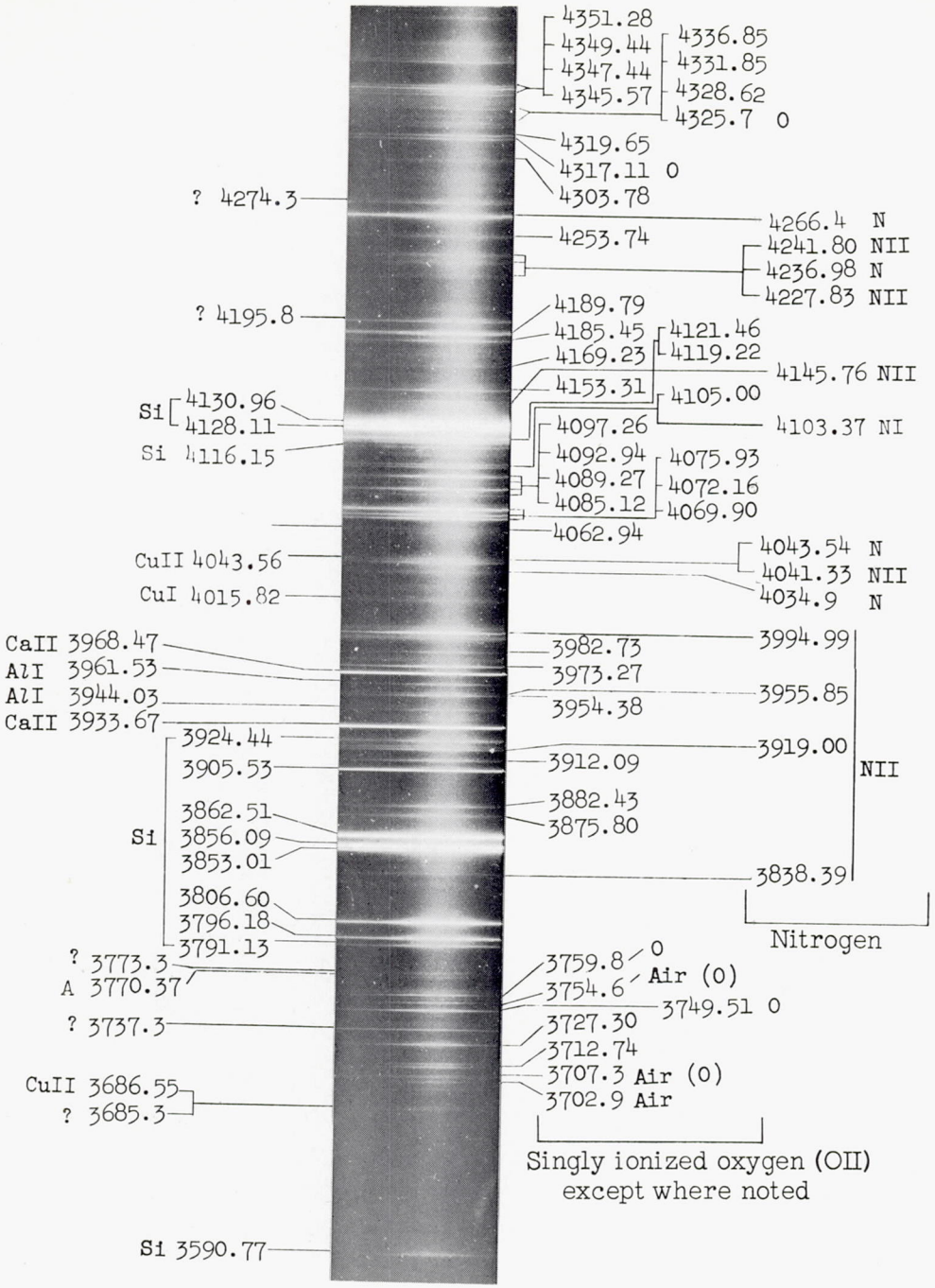

O	oxygen	Ca	calcium
N	nitrogen	Al	aluminum
A	argon	H_β	hydrogen beta line
Cu	copper	I	line classified as emitted by a normal atom
Si	silicon	II	line classified as emitted by a singly ionized atom

L-63-3192

Figure 16.- Identification of time-average spectrum of "air" radiation from discharge of pinch-tube generator in the range 3,590 A to 5,060 A.

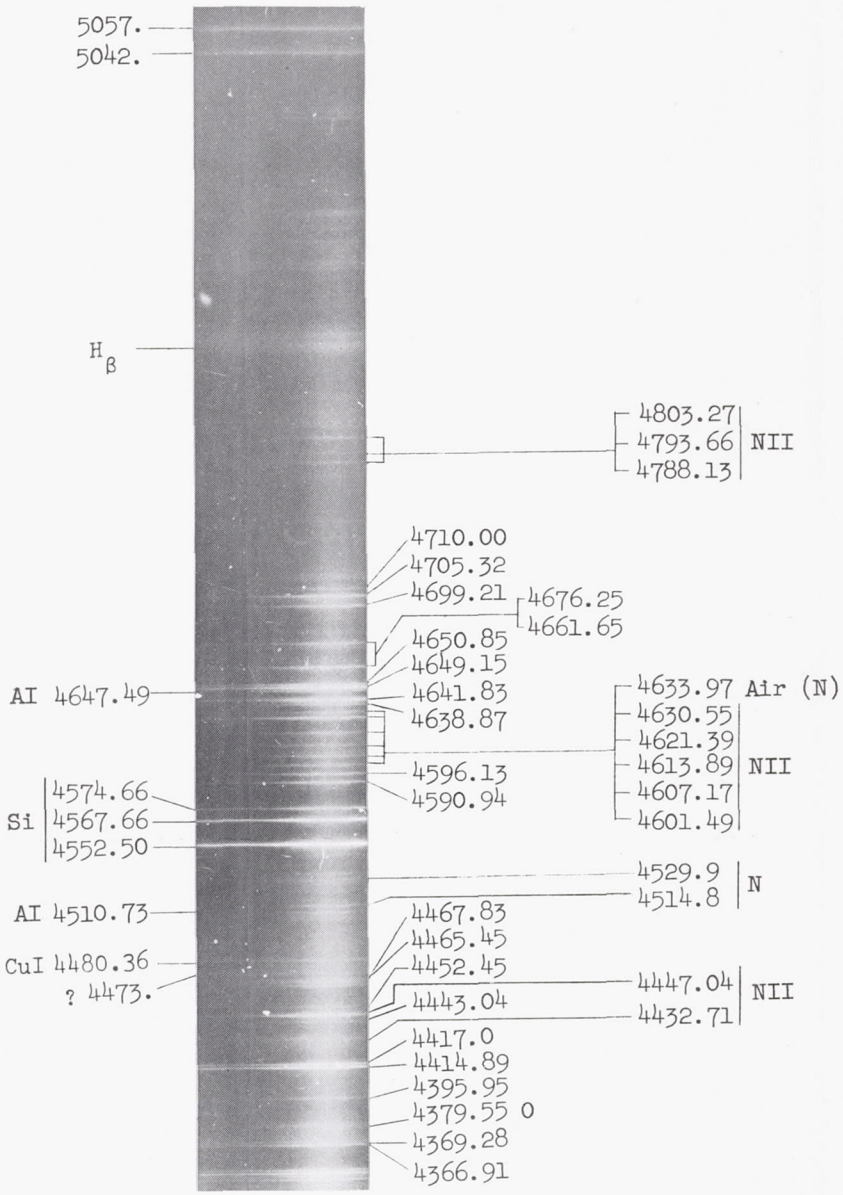

L-63-3193

Figure 16.- Concluded.